Remediation of AMD through bentonitic clay adsorption

HP Dannhauser

22146709

Dissertation submitted in fulfilment of the requirements for the degree *Magister* in Chemical Engineering at the Potchefstroom Campus of the North-West University

Supervisor: Prof FB Waanders

May 2016

Declaration

I, Hennus Dannhauser, hereby declare that the dissertation entitled

"Remediation of AMD through bentonitic clay adsorption"

submitted at the Potchefstroom campus of the North West University for the degree of Magister in Engineering, is completely my own work and that all resources used in compiling the report are referenced and acknowledged accordingly.

Signed on the _____ day of _____ 2015 at Potchefstroom.

_____

H. Dannhauser

Abstract

The discharge of acid mine drainage (AMD) from several abandoned mines in South-Africa has become a serious concern and environmental hazard. Since 2002 AMD has been decanting from the Number 8 shaft of the abandoned Harmony gold mine near Krugersdorp at 15-20 million litres per day. This acidic water, which contains high concentrations of metal ions in solution, has since contaminated a number of water sources in the surrounding area, including the Tweelopiespruit and several dams in the Krugersdorp game reserve.

The general method for treating AMD is by neutralising its acidity by the addition of a base compound such as lime or limestone. This method has proven to be rather ineffective, however, as iron ions present in the water can cause it to re-acidify once it has been released back into the environment. The use of lime and limestone to increase the pH of AMD also has an inherent drawback as it can lead to the formation of gypsum scaling which causes blockages of pipes and equipment, incurring additional costs for AMD processes.

Bentonite clay has received a lot of attention lately for its ability to adsorb a wide range of ions from solution, a trait which can be used to remove contaminants from AMD, and several AMD treatment methods and patents have been created based on this characteristic. An added advantage is that bentonite is readily available for large scale AMD treatment processes based on the number and output of bentonite mines in South Africa.

A study was undertaken to determine what effect the pH level of AMD has on the ability of bentonite to remove contaminants from it. Experiments were done where AMD samples collected from the Harmony AMD treatment site were treated with bentonite clay after the pH thereof had been altered by the addition of burnt dolomite powder, calcium hydroxide or magnesium hydroxide. The theory that burnt dolomite may be able to prevent the formation of gypsum was also investigated.

It was found that increased pH levels improved the removal efficiency of contaminants such as Fe, S and Al, though treatment at pH 7 is not advised as the shift from acidic to basic causes adsorption and precipitation to become erratic. Burnt dolomite powder was also found to be incapable of prompting gypsum precipitation as the magnesium content thereof precipitated too rapidly. The addition of pure magnesium hydroxide to the AMD did however decrease both Ca and SO_4^{2-} concentrations, indicating that it was successful in precipitating an amount of gyspum.

It is recommended that narrower pH ranges should be tested in future to further study the effects of pH on AMD treatment. A method to increase bentonite's adsorption capacity per weight unit by the removal of the clay's silica content should also be investigated. Polymers created by mixing bentonite clay with compounds such as $Ca(OH)_2$ and $CaCO_3$, as discussed by Ntwampe *et al.* (2015) also deserves further study as it shows promise for AMD treatment.

Keywords

Bentonite clay, Adsorption, Limestone, Dolomite, Acid mine drainage (AMD), Neutralize.

Opsomming

Die uitskeiding van suur myn water (AMD) vanaf verskeie myne wat nie meer operasioneel is in Suid Afrika nie wek ernsitge kommer en is ‘n ernstige gevaar vir die omgewing. Sedert die jaar 2002 word AMD daagliks teen byna 15-20 miljoen liter per dag uitgeskei vanaf die Nommer 8 mynskag van die verlate Harmony goud myn naby Krugersdorp. Hierdie suur water bevat hoë konsentrasies metaal ione in oplossing en het sedertdien ‘n aantal waterbronne in die omliggende area gekontamineer, onder andere die nabygeleë Tweelopiespruit en verskeie damme van die Krugersdorp wildreservaat.

Die algemene metode van AMD behandeling behels die neutralisering van die suurvlakke deur die byvoeging van ‘n basis soos kalk of kalksteen. Hierdie metode is egter oneffektief siende dat die yster ione wat teenwoordig is in die AMD kan veroorsaak dat die water terugkeer na ‘n suur toestand nadat dit vrygelaat word in die omgewing. Die gebruik van kalk en kalksteen het ook die nagevolg dat dit kan lei tot gips skalering wat blokkasies in pype en ander toerusting kan veroorsaak. Die verwydering van hierdie gips skalering kan lei tot addisionele kostes vir AMD behandelings prosesse.

Bentoniet klei besit die vermoë om ‘n wye reeks ione vanuit ‘n oplossing te adsorbeer. Hierdie eienskap kan gebruik word vir die verwydering van kontaminerende stowwe vanuit AMD, en verskeie metodes vir AMD behandeling is al ontwerp rondom die gebruik van bentoniet. ‘n Aantal bentoniet myne bestaan ook in Suid Afrika wat beteken dat bentoniet gereed beskikbaar is vir groot skaalse AMD behandelings prosesse.

‘n Studie is gedoen om te bepaal watse tipe effek die pH vlakke van AMD het op die vermoë van bentoniet om kontaminerende stowwe vanuit dit te verwyder. Eksperimente is uitgevoer wat die behandeling van AMD met bentoniet behels het nadat die pH van die AMD verander is deur die byvoeging van gebrande dolomiet poeier, kalsium hidroksied of magnesium hidroksied. Daar was ook getoets of die gebruik van dolomiet moontlik die formasie van gips skalering kan teenwerk.

Resultate het getoon dat verhoogde pH vlakke ‘n verbetering in die verwyderings effektiwiteit van kontaminante soos Fe, S en Al teweeg gebring het. Dit word egter nie aanbeveel dat AMD by ‘n pH van 7 behandel word nie, aangesien die oorgang vanaf ‘n suur na ‘n basiese medium onvoorspelbare gedrag veroorsaak aangaande adsorpsie en presipitasie reaksies. Gebrande dolomiet poeier is gewys om nie daartoe in staat te wees om gips presipitasie aan te moedig nie, omdat die magnesium inhoud daarvan te vinnig uit die oplossing presipiteer.

Dit word aanbeveel dat toekomstige projekte nouer pH reekse moet toets sodat die effekte van pH verder ondersoek kan word. ‘n Metode om bentoniet se adsorpsie kapasiteit te verhoog deur die silika inhoud daarvan te verwyder moet ook ondersoek word. Verder is dit ook belangrik dat die polimere wat beskryf is deur Ntwampe *et al.* (2015), wat gevorm word deur mengsels van bentoniet, $Ca(OH)_2$, $CaCO_3$, en ander stowwe, verder nagevors word aangesien dit belowend kan wees vir AMD behandeling.

Sleutelwoorde

Bentoniet klei, Adsorpsie, Kalksteen, Dolomiet, Suur myn water (AMD), Neutraliseer.

Acknowledgements

I would like to thank the following persons for their support and contributions during the completion of this project:

- My project leader, Professor Frans Waanders, for his advice, guidance, assistance and patience, and without whom this project could not have realised
- Mr Ntwampe for his willingness to sacrifice his own time to provide assistance and impart knowledge
- My parents and family, for their love, support and prayers throughout the entire year, and for always believing in me
- Simoné Botha, for her love, encouragement and support throughout the project
- I thank God for the blessings He has bestowed upon me and for giving me the strength and skills which I needed to complete this project

The information presented in this paper is based on the research that is partially financially supported by the South African Research Chairs Initiative (SARChI) of the Department of Science and Technology and National Research Foundation of South Africa (Coal Research Chair Grant No. 86880).

Any opinion, finding, conclusion or recommendation expressed in this material is that of the author(s) and the NRF does not accept any liability in this regard.

Contents

List of figures

List of tables

List of abbreviations and acronyms

ACE	Associated Chemical Enterprises
AMD	Acid Mine Drainage
ARD	Acid Rock Drainage
CCM	Constant Capacity Model
CEC	Cation Exchange Capacity
DLM	Diffuse Layer Model
ECCM	Extended Constant Capacity Model
ICP-MS	Inductively Coupled Plasma Mass Spectrometry
ICP-OES	Inductively Coupled Plasma Optical Emission Spectrometry
NTU	Nephelometric Turbidity Units
PPM	Parts Per Million
RF	Radio Frequency
RPM	Revolutions Per Minute
SCM	Surface Complexation Model
TDS	Total Dissolved Solids
TLM	Triple Layer Model
T-O-T	Tetrahedral-octahedral-tetrahedral
XRD	X-Ray Diffraction
XRF	X-Ray Fluorescence

Chapter 1 : Introduction

1.1 Background

The South African mining industry is one of the largest in the world due to the country's abundant mineral resources (Kearney, 2012). In recent years the mining of gold has started to decline, but the mining of other rare earth metals and elements is likely to continue in the foreseeable future. Whilst mining is of great importance to South Africa, it is challenged by inherent environmental risks and associated problems (Oelofse & Strydom, 2010). The formation of acid mine drainage (AMD) is one of the most critical issues to address as it has a major environmental impact on the scarce water resources in South Africa. (Oelofse & Strydom, 2010).

During mining operations, and sometimes after these operations have stopped, sulphide minerals such as pyrite (FeS_2) can become oxidised in the presence of water. As a result of this oxidation, a strong acid is formed which is referred to as acid main drainage (AMD) (Gitari et al., 2011). Because of the high acidity of AMD (pH varying between 2-4), metals, sulphides and other elements are at risk of being leached out of the surrounding rock by the AMD. As such, AMD usually also contains fair concentrations of rare earth elements and metals (Heviánková et al., 2014).

AMD can contaminate surrounding bodies of water, such as groundwater, rivers or lakes, which can lead to the death of wildlife and making it unsuitable for human consumption (Jennings et al., 2008). In South Africa, AMD first became a problem in 2002 when a flooded underground mine on the West Rand started discharging large amounts of AMD into the environment. As stated, water is a scarce resource in South Africa that has to be reserved for our current and future generations. Therefore the topic of how to deal with AMD has received a lot of attention since then and research into methods of dealing with AMD has increased significantly (Oelofse & Strydom, 2010).

The most effective way of dealing with AMD is to neutralise its acidity to make it safe for use once again. A technique for achieving this is by manipulating the pH of the AMD and using bentonite clay to adsorb the contaminating elements which precipitate from the water (Gitari et al., 2011). When using this process, one is left with bentonite clay which is loaded with heavy metals and traces of other rare earth elements. It is however possible to recover these metals from the clay through leaching (Enslin et al., 2010), making the clay re-usable and providing a potential source for the recovery of rare elements and metals (Gitari et al., 2011).

1.2 Objective and aim of the study

The main objective of this project is to determine the effect that pH level has on the ability of bentonite to treat AMD water effectively. Additionally, as a secondary objective it also aims to determine if burnt dolomite is a viable compound for pH control during AMD treatment and, if the use thereof can decrease the formation of calcium sulphate which causes scaling in piping and other equipment. Thirdly, pure Calcium hydroxide and Magnesium hydroxide will be used individually for pH adjustment to test their effectiveness and compare it with that of dolomite, which contains both of these compounds. The testing will be done through laboratory experimentation, and by analysing the experimental results, the intention is to determine the best conditions for the treatment and remediation of AMD with the use of bentonite clay and to determine if it is a viable process for AMD treatment.

Chapter 2 : Literature survey

2.1 Acid mine drainage (AMD)

Acid rock drainage (ARD) is an acidic fluid which is produced when sulphide minerals, such as iron pyrite (FeS_2), undergo oxidation. This chemical reaction occurs naturally when water and air come into contact with these minerals (Gitari et al., 2011). In nature this process occurs over long periods of time and at very slow rates, enabling the environment to buffer the effects of the produced acid (Maicaneanu et al., 2013). Activities such as mining however increases the quantity of exposed sulphur-bearing rock for oxidation, leading to the generation of large amounts of acid which exceeds nature's buffering ability. Acid water formed from sulphide bearing rock as a result of mining activity is referred to as Acid Mine Drainage (AMD) (Maicaneanu et al., 2013).

2.1.1 AMD formation

When pyrite is oxidised in the presence of water the result is the formation of hydrogen ions, sulphate ions and soluble metal ions, causing the water to become acidic (Jennings et al., 2008).

$$4FeS_2(s) + 14O_2(g) + 4H_2O(l) \rightarrow 4Fe^{2+}(aq) + 8SO_4^{2-}(aq) + 8H^+(aq) \quad \text{(Eq. 1)}$$

If sufficient oxygen is present, ferrous iron (Fe^{+2}) can undergo further oxidation to form ferric iron (Fe^{+3}).

$$4Fe^{2+}(aq) + O_2(g) + 4H^+(aq) \rightarrow 4Fe^{3+}(aq) + 2H_2O(l) \quad \text{(Eq. 2)}$$

From here the ferric iron can form ferric hydroxide ($Fe(OH)_3$) which precipitates in the water as a visible red-orange solid (Eq. 3), clearly visible in Figure 2.1. It can also react further with pyrite to form more ferrous iron, hydrogen ions and sulphate ions, leading to a further increase in the water's acidity and even faster oxidation (Eq. 4) (Jennings et al., 2008).

$$4Fe^{3+}(aq) + 12H_2O(l) \rightarrow 4Fe(OH)_3(s) + 12H^+(aq) \quad \text{(Eq. 3)}$$

$$14Fe^{3+}(aq) + FeS_2(s) + 8H_2O(l) \rightarrow 2SO_4^{2-}(aq) + 15Fe^{2+}(aq) + 16H^+(aq) \quad \text{(Eq. 4)}$$

This process continues as long as a source such as pyrite is present for oxidation. In time the pyrite becomes fully oxidised and AMD generation ceases, however this takes a long period of time and can possibly take decades or even centuries (McCarthy, 2011).

Figure 2.1: AMD decant with visible red-orange discoloration (Waanders, 2015)

2.1.2 AMD and the environment

As mentioned before, certain mining operations can cause large amounts of sulphur bearing rock to be exposed to the elements, forming AMD at a rate faster than is manageable by natural means (Maicaneanu et al., 2013). Large amounts of acidic liquid being released into natural surroundings can have serious environmental and biological implications (Jennings et al., 2008).

AMD has a pH varying between 2 and 4 (Heviánková et al., 2014) and when coming into contact with fresh water bodies it can lower the pH thereof to levels where the water becomes unsuitable for domestic use and incapable of supporting aquatic life (McCarthy et al., 2010). Lowering the pH and making the water more acidic also enables the water to liberate certain metals, including radioactive nuclides and toxic metals, from surrounding rock bodies. At high enough levels these elements can cause the water to become severely toxic to humans, animals and the environment (Coetzee et al., 2006). The pH of AMD is not as high as that of concentrated acids, giving it a lower level of corrosivity. However, certain materials can still be affected or damaged by it over long terms of exposure (McCarthy et al., 2010).

The reactions which take place during the formation of AMD also leave water with a high sulphate level. Even after the water is neutralised and the pH returned to normal, the

sulphates will remain at these levels. Sulphates also increase the salinity of the water which can make it unusable for agricultural, domestic or industrial use (McCarthy et al., 2010).

2.1.3 AMD issues in South Africa

South Africa has a very large mining industry (Kearney, 2012), and it is therefore no surprise that certain areas within South Africa have also reported problems concerning AMD. The areas of most concern include the O'Kiep copper district, the coal fields in Mpumalanga and KwaZulu-Natal, and the Witwatersrand gold fields (McCarthy et al., 2010). In these areas flooding of the mines has led to the discharge of AMD into the environment, which in turn has caused contamination of shallow groundwater resources and major river systems in the surrounding area, such as the Olifants and Vaal river systems (McCarthy et al., 2010). In a country such as South Africa, where water is already a scarce resource, the contamination of any body of fresh water is of serious concern (Ewart, 2011).

Since 1886, when gold was discovered in the Witwatersrand area, the three underground basins (large developments of connected mines) of the East-, Central- and West Rand have been subject to mining operations. Whilst still in operation, water was pumped from these mines continuously to prevent flooding and allow access to the underground gold reserves (South African Department of Water & Sanitation, 2015). After these mines were worked out however and operations ceased, the mines were abandoned and pumping was stopped. Over time the voids left by these mines, such as shafts and tunnels, filled up with water and became flooded (Scott, 1995). Sulphide rich rock surfaces, uncovered as a result of the mining operations, coming into contact with this water led to the formation of millions of litres of AMD within the abandoned mines (Scott, 1995). Figure 2.2 shows the geographic locations of the Witwatersrand basins.

The Western and Central basins of the Witwatersrand have no more mines in operation, and therefore no water is pumped from these mines anymore, leading to increasing levels of flooding within these abandoned mines (Scott, 1995). The contaminated water from these mines inevitably start to discharge and flow into domestic water supplies. AMD pollution of the Wonderfontuinspruit catchment area has been an on-going concern since 1967, and many dams along the Wonderfontuinspruit and Mooi Rivier catchment area contain high contaminant concentrations (Brink, 2009). In August of 2002, AMD contaminated water began to decant from the Western basin, around the Krugerdorp area, from the abandoned Number 8 shaft of Harmony Gold Mining Company, into the surface environment. The AMD

from this shaft is discharged at a rate of 15-20 megalitres per day (Ml/d), peaking at about 60 Ml/d during rainfall seasons (McCarthy et al., 2010).

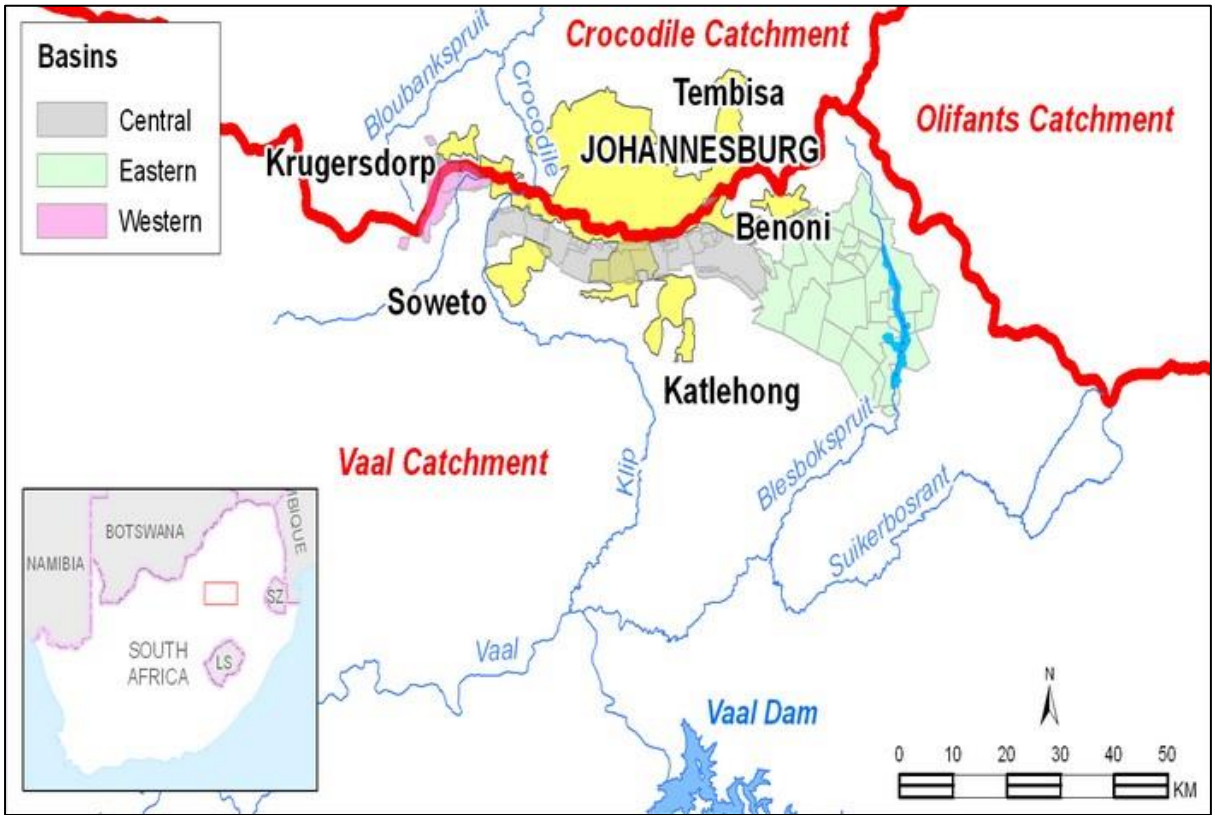

Figure 2.2: Map of the Witwatersrand showing the West, Central and East mining basins (South African Department of Water & Sanitation, 2015)

2.1.4 The Krugersdorp AMD situation

Raw AMD has continuously been discharging from the abandoned number 8 shaft of the Harmony Gold Mining Company near Krugersdorp since 2002, causing severe environmental damage (McCarthy et al., 2010). This section will serve to explain how this problem evolved, as well as the consequences thereof. Refer to Figure 2.3 for visual details.

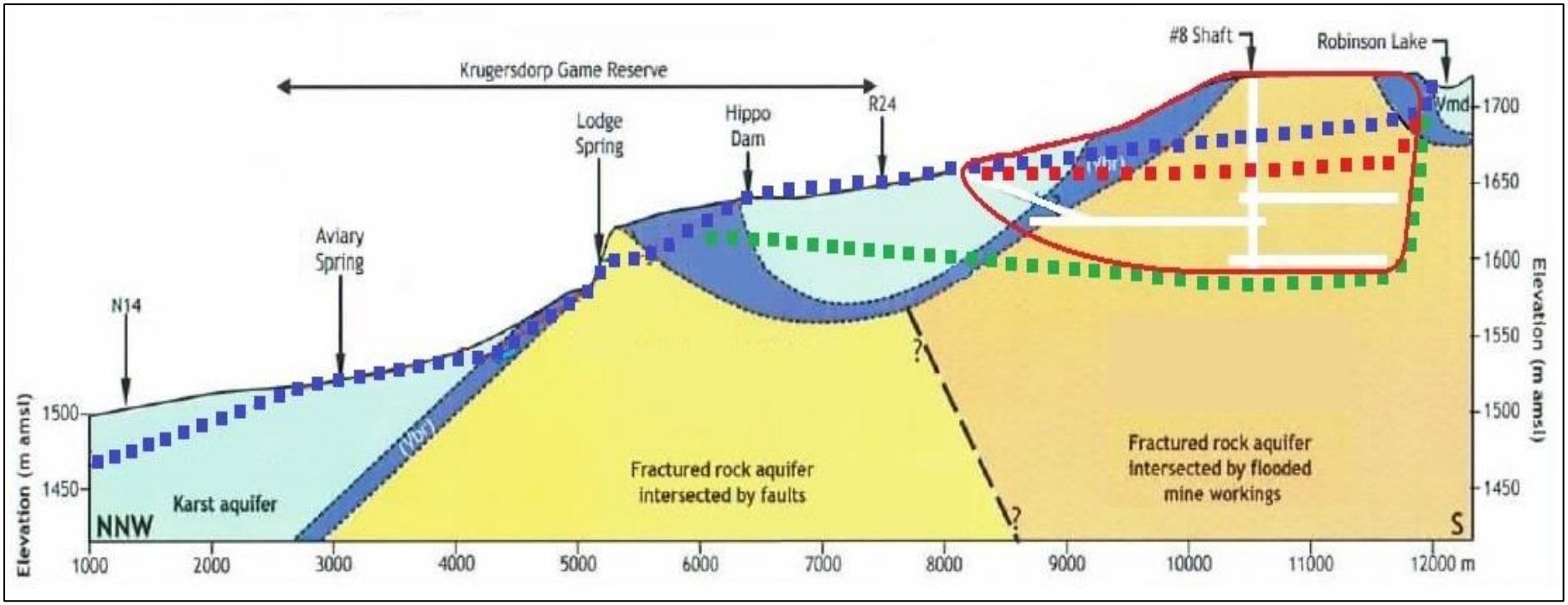

Figure 2.3: Hydrogeological profiles of the Krugersdorp area showing the piezometric surface before (■), during (■) and after (■) mining operations (Modified from Coetzee, 2009)

Before mining started, the water table would have followed a natural piezometric surface, as indicated by the blue dotted line on Figure 2.3. In areas where the piezometric surface lies above ground level springs could form if a suitable conduit existed by which water could flow to the surface. Once mining started (White lined areas on Figure 2.3) water was continuously pumped from the shafts and tunnels of the mine, causing the water table to lower in the area surrounding the mine. All springs within this area which was located above the level of the new water table, shown by the green dotted line on Figure 2.3, would have dried up because of dewatering. When mining operations were halted, the pumping of water from the shafts and tunnels were stopped, which allowed the water table to start rising again back to its original level. Due to the higher transmissivity of the mined out voids however this level was now lower than before as indicated by the red dotted line on Figure 2.3. The empty mining tunnels and shafts, now filled with water, created an AMD generation zone (Red encircled area on Figure 2.3) where water could freely react with the exposed sulphur-bearing rocks and become acidic, contaminating the surrounding groundwater. As before, water, now contaminated and acidified, began to decant from conduits and openings below the piezometric surface into the surrounding wetlands, draining into the Tweelopiespruit (Coetzee, 2009). The Tweelopiespruit flows into the Krugersdorp game reserve, where it has contaminated the park's hippo dam, aviary dam and the natural springs to great extent. Figure 2.4 shows the Tweelopiespruit and the outflow of the game reserve's aviary dam. In both photos the signature red-orange colouring is clearly visible, indicating high levels of iron in the water (Earthlife Africa, 2015).

Figure 2.4: Right: The AMD contaminated Tweelopiespruit flowing under the R24 road into the Krugersdorp game reserve. Left: Water flowing out of the game reserve's aviary dam showing clear signs of contamination (Earthlife Africa, 2015).

2.1.5 AMD treatment

Currently the most widely used method for treating AMD is by simply neutralising its acidity, usually by the addition of an alkali such as limestone ($CaCO_3$), which is readily available (Brink, 2009). This method is ineffective however since Fe^{3+} ions which are reduced to Fe^{2+} by the increase in pH will re-oxidise to the Fe^{3+} state when coming into contact with air. This re-oxidation causes sulphuric acid to be formed once again, returning the previously neutralised AMD back to an acidic state (Brink, 2009). Brink (2009) found that AMD which had been neutralised and treated to fulfil environmental laws would acidify again after a short time of being released into the environment. To completely neutralise and purify the AMD, the pH must be raised to a high enough level where iron ions can precipitate and be removed from the water to prevent acidification from reoccurring (Brink, 2009).

The insolubility of heavy metals in alkaline conditions is the source of AMD neutralisation through precipitation. When raising the pH of the AMD to around 9.5, metals such as copper (Cu), zinc (Zn) and most importantly iron (Fe) will start to precipitate. If the pH is raised further to between 10.5 and 11, metals such as cadmium (Cd) and nickel (Ni) will precipitate as well, as shown in Figure 2.5 (Aubé, 2004).

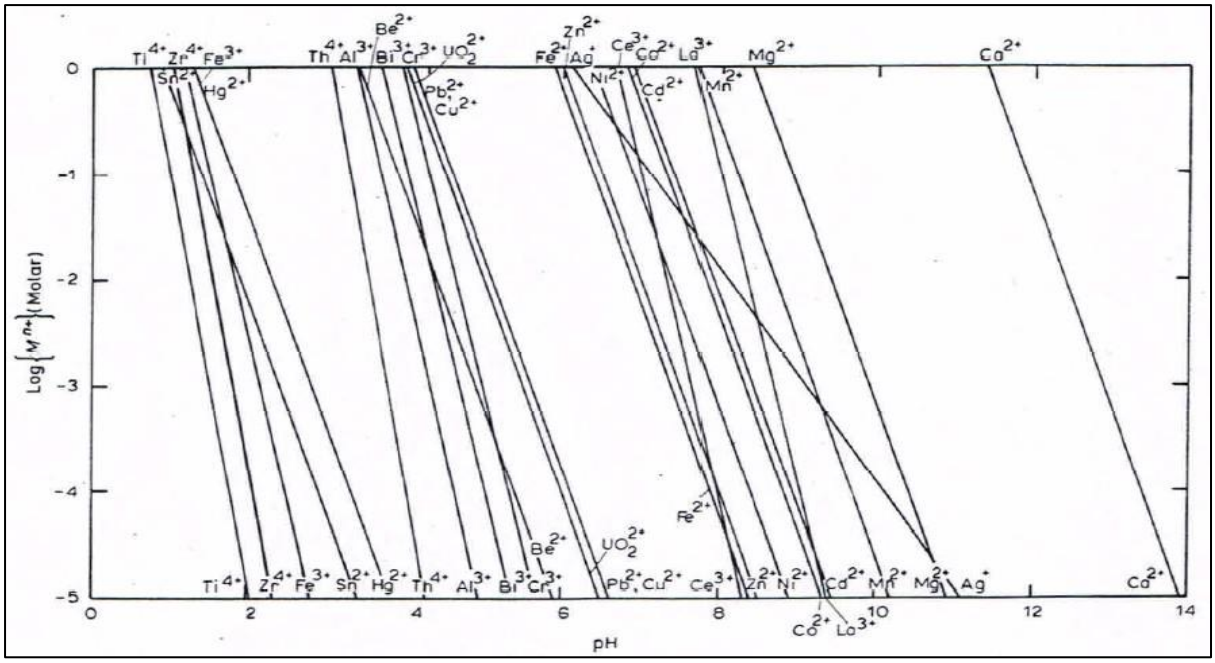

Figure 2.5: Monhemius metal hydroxide precipitation diagram (Zinck, 2005)

The conventional way of treating AMD through precipitation is with the use of lime (CaO) to increase the pH levels instead of normal limestone. This is due to the fact that limestone is inefficient when dealing with sulphuric acid because of a buffering effect which occurs. Brink (2009) performed an experiment to show this effect by adding limestone to water which had been acidified by sulphuric acid to a pH of 0.95. The results (Figure 2.6) showed that once a pH level of ≈6 was reached the effectiveness of the limestone drastically decreased and a pH of 7 or higher could not be reached, indicating that additional processes must be used to obtain higher pH levels (Brink, 2009)

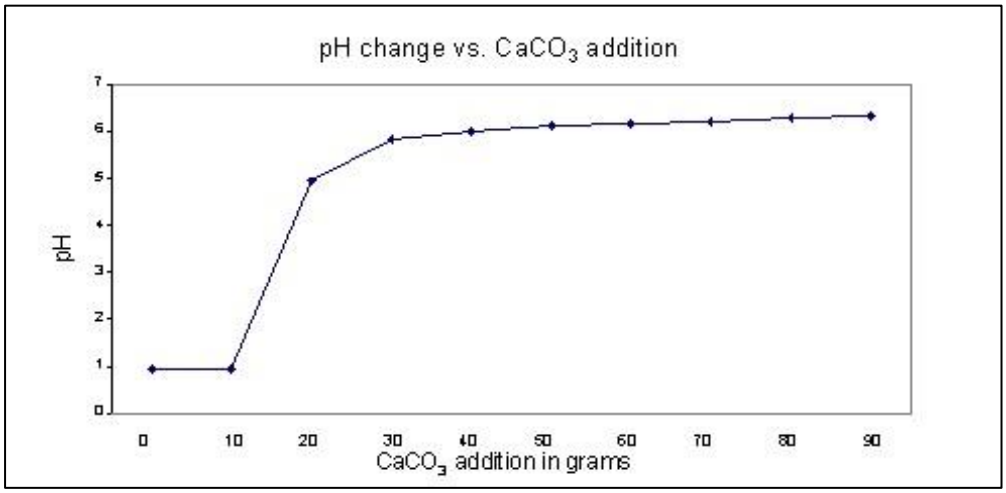

Figure 2.6: Graph of pH change in acidic water from limestone addition (Brink, 2009)

Lime is produced by heating limestone to temperatures of 900°C or above, causing carbon dioxide gas to be released from the limestone (Equation 5). This process is referred to as limestone calcination or burning (Ispat Digest, 2014).

Figure 2.7 shows the difference in appearance between normal limestone and limestone which has been calcined to form lime.

$$CaCO_3 + Heat \rightarrow CaO + CO_2 \quad \text{(Eq. 5)}$$

Figure 2.7: Visual comparison of Limestone (Left) and Lime (Right) (Lhoist, 2015)

Controlling the pH using burnt lime requires that the lime first has to be slaked or hydrated by the addition of water. An increase in pH occurs when the slaked lime dissolves and forms hydroxide ions according to equations 6 and 7 (Aubé, 2004).

$$CaO + H_2O \rightarrow Ca(OH)_2 \quad \text{(Eq. 6)}$$

$$Ca(OH)_2 \rightarrow Ca^{2+} + 2OH^- \quad \text{(Eq. 7)}$$

When slaked lime is added to AMD, the hydroxide ions and dissolved metals combine to produce precipitates which can settle down to form a sludge at the bottom of the tank or container in which the AMD is being treated. Equations 8 to 11 show how some of the dissolved metals form precipitates by combining with the hydroxide ions (Aubé, 2004).

$$Fe^{2+} + 2OH^- \rightarrow Fe(OH)_2 \quad \text{(Eq. 8)}$$

$$Fe^{3+} + 3OH^- \rightarrow Fe(OH)_3 \quad \text{(Eq. 9)}$$

$$Al^{3+} + 3OH^- \rightarrow Cu(OH)_3 \quad \text{(Eq. 10)}$$

$$Cu^{2+} + 2OH^- \rightarrow Cu(OH)_2 \quad \text{(Eq. 11)}$$

After settling of the metal precipitates has occurred, the clear upper layer of water, which has now been neutralized and stripped of dissolved metals, can be recovered and either released directly to the environment or sent for further treatment. There are two main treatment processes based on this principle, namely the pond treatment and the conventional treatment plant (Aubé, 2004).

A treatment pond (Figure 2.8) is an inexpensive and simplistic treatment method which involves the addition of slaked lime into an AMD stream which flows to a settling pond. Here the precipitates are allowed to settle and the treated effluent is allowed to flow out. This method allows for large quantities of AMD to be treated but a very large surface area is required for the settling ponds and regular draining of the ponds are required to clear the build-up of precipitated sludge. The efficiency of the added lime is also very low with this method since there is no form of mechanical mixing with the lime being added in stream and being left to mix naturally (Aubé, 2004).

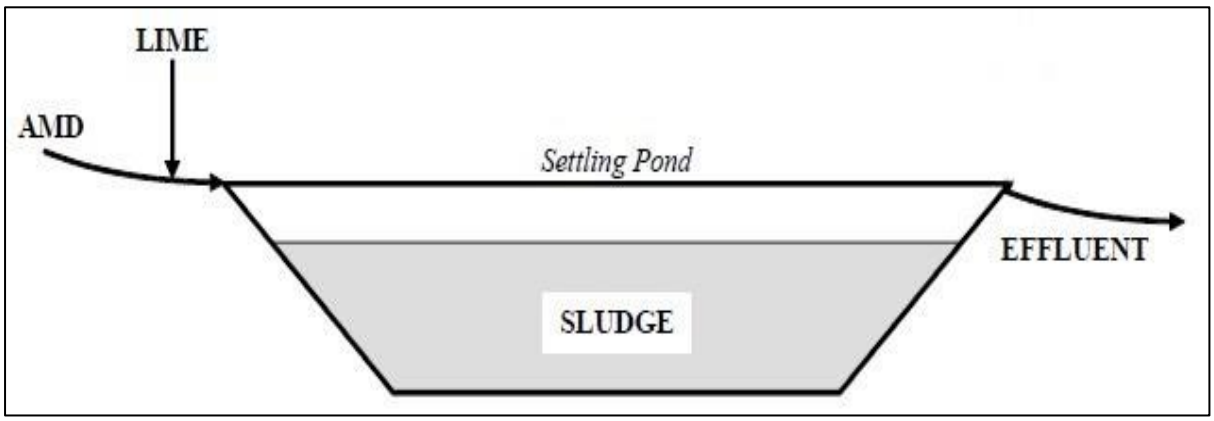

Figure 2.8: Pond treatment of AMD (Aubé, 2004)

Ferrous hydroxide ($Fe(OH)_2$) is not as stable a compound as ferric hydroxide ($Fe(OH)_3$) and does not settle as well when precipitating. For this reason conventional treatment plants sometimes aerate the AMD and hydrated lime mixture in a lime reactor to fully oxidise the ferrous hydroxide into the more stable ferric hydroxide, as shown in Equation 12 (Aubé, 2004).

$$4Fe(OH)_2 + 2H_2O + O_2 \rightarrow 4Fe(OH)_3 \qquad \text{(Eq. 12)}$$

From the lime reactor the mixture is sent so a clarifier where settling can occur. A flocculant is also added to the mixture to speed up the settling process. This method is more efficient than the pond treatment since better mixing of the lime and AMD occurs and the pH levels can be more easily controlled. The use of clarifiers also allows continuous removal of sludge

during operation, negating the need to drain the settling tanks for sludge removal (Aubé, 2004). Figure 2.9 shows the basic layout of a conventional treatment plant.

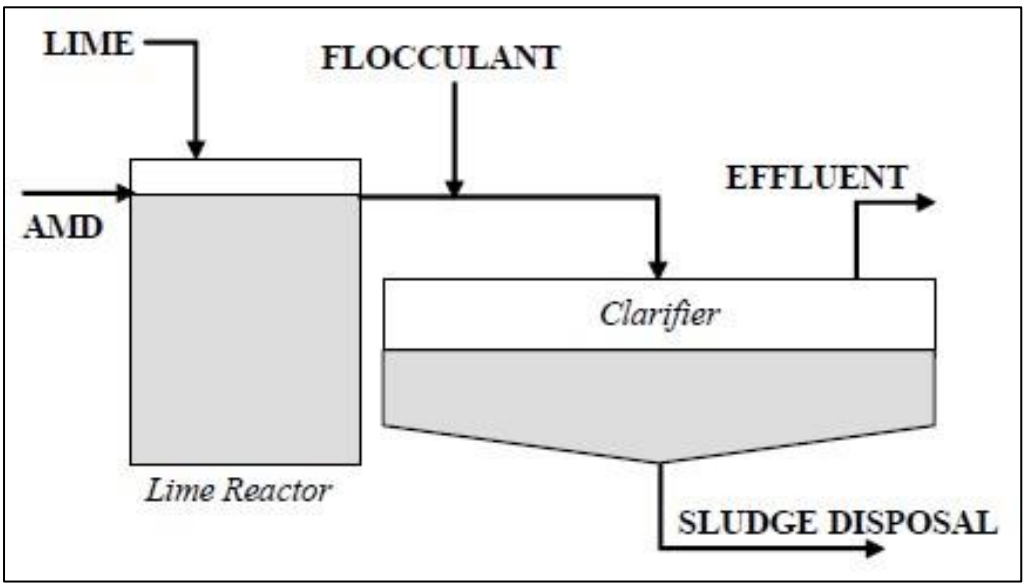

Figure 2.9: Conventional AMD treatment plant (Aubé, 2004).

2.1.6 Harmony AMD treatment plant

Harmony Gold Mining Company Ltd., the third largest gold mining company in South Africa, has a large scale AMD treatment site at Tweelopiespruit near Krugersdorp. This site, marked site A on Figure 2.10, treats the large volumes of AMD originating from the old abandoned Number 8 mine shaft as discussed in section 2.1.4. AMD which decants from this shaft flows directly into a holdings dam, site B on Figure 2.10, from where it is pumped to treatment pits at the treatment site. Here a large volume of limestone, which is acquired as a waste product from the paper manufacturing industry, is added to the AMD to raise the pH thereof. In addition to the limestone, slaked lime is also used to raise the pH sufficiently for metal precipitation to occur. Settling of precipitates and other solids is allowed to take place to some extent and the effluent flows over into a second pit from where it is released into the Tweelopiespruit. Photos of the treatment site are shown in Figures 2.11 to 2.13.

Figure 2.10: Map view of Tweelopiespruit area showing the Harmony AMD treatment plant (A), AMD holdings dam (B) and the void (C) in relation to one another

Figure 2.11: Harmony gold mining company's Tweelopiespruit AMD treatment site (Waanders, 2015)

Figure 2.12: Treatment pit with raw AMD before limestone addition (Waanders, 2015)

Figure 2.13: Treatment pit with AMD after limestone addition and settling has occurred (Waanders, 2015)

In recent years Harmony has changed the treatment process somewhat to include a recycling system. After the initial limestone treatment and settling, only part of the treated AMD effluent is released into the environment while the remainder is sent to the void, site C on Figure 2.10, where it mixes with the raw untreated AMD deposited there. The void is an old opencast mine which has been filled by AMD decant over time. Through the interconnection of old mining tunnels, the AMD from the void eventually also decants from the number 8 shaft and flows into the holdings dam at site B, from where it is once again sent to the treatment site. By changing the process as described and recycling part of the treated water, Harmony has created a semi-closed system and the mixing of already treated AMD with the raw deposits from the void has led to decreased levels of contamination within the AMD decanting from the number 8 shaft. Figure 2.14 shows the concentrations of some elements found in a sample taken from the site B holdings dam in February of 2014 in comparison with levels from a sample taken in September 2015. The readings from a sample taken by Brink in 2009 from the same dam are also shown. At the time this sample was taken the recycle of treated AMD had not yet been implemented.

The sample taken by Brink (2009) contains practically no traces of calcium or magnesium, indicating that the AMD had not been neutralized in any way by the addition of alkaline compounds at this point and it was truly raw AMD decanting from the number 8 mine shaft. Since Brink's sample was taken in 2009 and the recycle step of the treated AMD was implemented in the treatment process, calcium and magnesium concentrations in the AMD decant has increased whilst iron and sulphate levels have both decreased by nearly 99%.

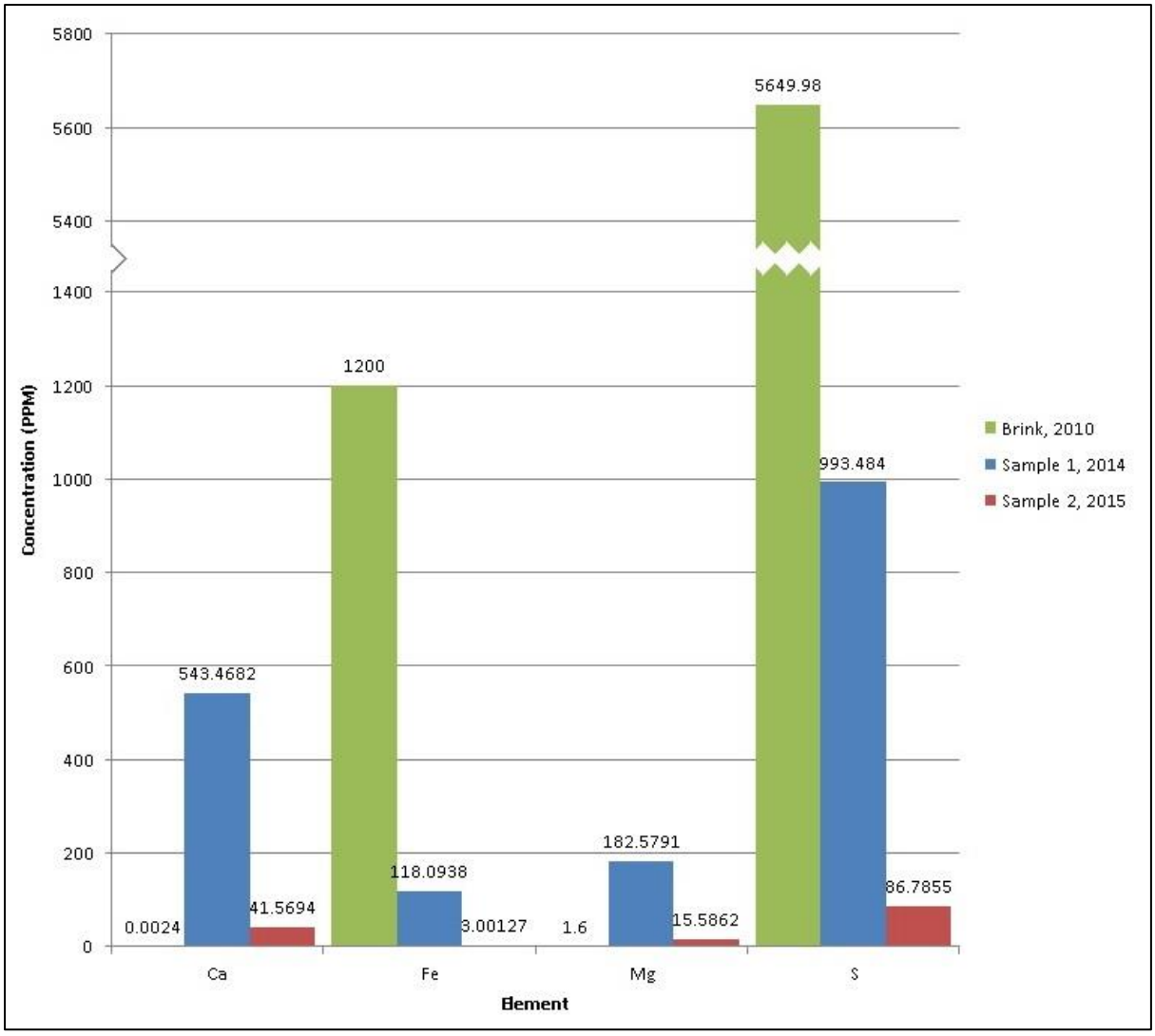

Figure 2.14: Graph comparing concentrations of some elements in AMD samples taken in 2014 and 2015 at Harmony mining's Tweelopiespruit treatment site (With S = SO_4^{2-} ion concentration)

2.2 Lime scaling

As stated in section 2.1.5, AMD treatment is largely dependent on lime addition for pH control. There is however a disadvantage to this as it often leads to lime scaling issues. Scaling occurs due to the formation of gypsum ($CaSO_4.2H_2O$) when slaked lime is added to sulphate rich water, such as AMD, which brings the solubility product above saturation (Zinck, 2005).

$$Ca(OH)_2 + H_2SO_4 \rightarrow CaSO_4 \cdot 2H_2O \qquad \text{(Eq. 13)}$$

Once the saturation point is reached, gypsum will start to precipitate and crystalize onto the walls of tanks and pipes. Once this occurs, gypsum precipitation and crystallization will start to increase since gypsum crystals form more easily on already existing gypsum (Zinck,

2005). Gypsum formation is a very slow process, and it is this slowness which causes it to be a problem. Metal precipitation from AMD occurs very rapidly, while gypsum formation can take days to occur. Because of this, effluent is often pumped from settling tanks while still being saturated by gypsum, causing effluent systems such as clarifier overflow weirs and piping to become covered in gypsum scale, resulting in blockages (Aubé, 2004). Figure 2.15 shows a pipe with scale build-up.

Figure 2.15: Scale build-up within a pipe (Envirofluid, 2014)

Removing gypsum from solid surfaces is very difficult as it is a very hard scale which adheres tightly to surfaces. In some cases, such as in Figure 2.15 it is more cost effective to simply replace piping in which severe scaling has occurred rather than trying to remove the gypsum. Gypsum scaling is thus a very large problem which can cause increased and unwanted costs for AMD treatment processes (Zinck, 2005). It is however possible to solve this problem through the added use of magnesium compounds, as shown by Brink (2012), due to a principle known as the common ion effect. This will be discussed further in section 2.3.

2.3 The common ion effect

The common ion effect describes the effect which a substance has on an equilibrium reaction by adding an ion which is already part of the reaction. The common ion effect is better understood by first looking at Le Chatelier's principle (Culgor, 2014).

Le Chatelier's principle states that if the conditions in a system which is at equilibrium is changed and the equilibrium disturbed, the equilibrium will shift in order to counter this change and re-establish the balance (William et al., 2007).

To illustrate this, an example will be given based on a saturated solution of calcium carbonate, the equilibrium reaction of which is shown in Equation 14.

$$CaCO_3(s) \rightleftharpoons Ca^{2+}(aq) + CO_3^{2-}(aq) \qquad \text{(Eq. 14)}$$

Being at equilibrium, ions are constantly being formed while calcium carbonate is being precipitated at rates which balance each other out. If an amount of calcium chloride ($CaCl_2$), which has a higher solubility than $CaCO_3$, is now added to the solution it will dissociate into calcium and chloride ions.

$$CaCl_2(s) \dashrightarrow Ca^{2+}(aq) + 2Cl^{-}(aq) \qquad \text{(Eq. 15)}$$

The addition of the calcium chloride thus causes the concentration of Ca^{2+} ions in solution to increase, which in turn disturbs the equilibrium of equation 14 and causes it to shift to the left. When the equilibrium shifts leftwards, more $CaCO_3$ will be formed while the concentration of CO_3^{2+} ions will decrease. By adding a compound which forms an ion which is common to one of the ions already in solution, in this case the Ca^{2+} ion, the solubility of the compound already in solution thus becomes decreased and it will start to precipitate. This is the basic principle of the common ion effect (Culgor, 2014).

This principle can be applied to solve the problem of gypsum formation from slaked lime during AMD treatment, as shown by Brink (2012). By adding magnesium to AMD after it has been treated with slaked lime, magnesium sulphate ($MgSO_4$) is formed, which has a higher solubility than $CaSO_4$. This causes the SO_4^{2-} ion concentration to increase and due to the common ion effect, as described above, $CaSO_4$ is precipitated. After the precipitation of the calcium sulphate, magnesium sulphate will remain in the water. However this can be removed by bentonite addition and adsorption to yield clean water (Brink, 2012).

2.4 Bentonite clay

Named after Fort Benton, located in Wyoming (USA), near to where it was first discovered, bentonite clay was first mined in 1897 (Enslin, 2009). Since then bentonite has become widely used in many industries such as agriculture, cosmetics, drilling, civil engineering and for use as catalysts and adsorbents (Van der Wat, 2011). The adsorbent qualities of bentonite are instrumental for achieving the objectives of this project. Bentonite is an excellent compound for use in AMD treatment, as was shown by Brink in 2009 and 2012 when he used bentonite clay to remove dissolved metal ions from AMD.

2.4.1 Bentonite characteristics

Bentonite is a plastic clay which is naturally formed by the alteration of siliceous, glass-rich volcanic ash. Natural weathering of some silica bearing rocks such as basalt and granite can also lead to bentonite formation. Due to the hydrological environment in which the formation takes place, and because of climatic differences, most bentonite deposits are unique and vary in their elemental composition from location to location (Vermeulen, 2012). Bentonite clay is normally named for the main trace mineral element within its structure, such as sodium (Na) bentonite and calcium (Ca) bentonite. Clay which contains both sodium and calcium is simply referred to as bentonite (European Bentonite Producers Association, 2015)

Despite the different chemical compositions of bentonite deposits, all bentonite clays have mineral montmorillonite as their main component. Montmorillonite containing clays are part of the smectite mineral group. Smectites are clay minerals which have a layered structure of individual crystallites and have high cation-exchange capacities as well as swelling properties. Two types of smectite groups exist, namely Trioctahedral and Dioctahedral smectites (Vermeulen, 2012). Montmorillonite smectites are classified as dioctahedral smectites, as is shown in Figure 2.16.

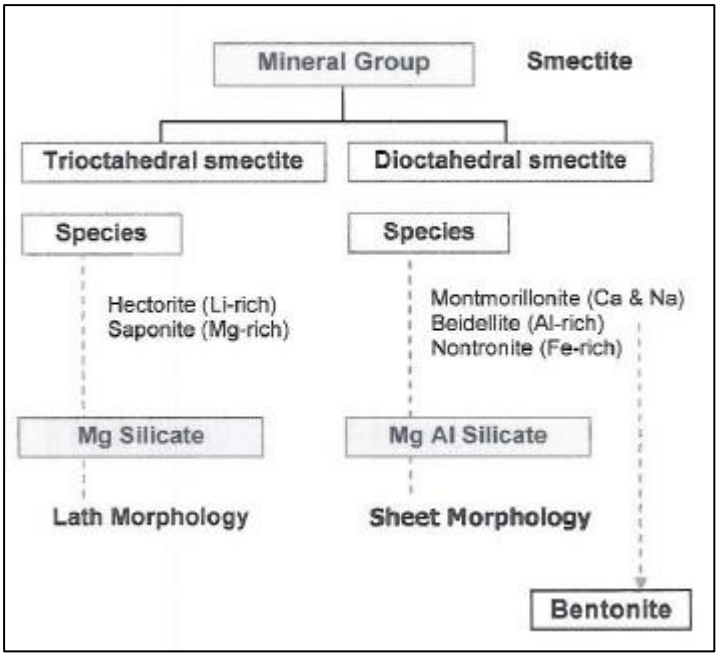

Figure 2.16: Smectite classification (Vermeulen, 2012)

Smectite crystallites are normally no larger than 2µm and are three-layer clay minerals consisting of an octahedral layer and two tetrahedral layers (European Bentonite Producers Association, 2015). Montmorillonite's structure consists of a central $Al(O_5,OH)$-octahedron layer (where Al can also be either magnesium or in some cases iron) enclosed by two SiO_4-tetrahedron layers, creating a tetrahedral-octahedral-tetrahedral (t-o-t) aluminosilicate sheet (European Bentonite Producers Association, 2015). The molecular structure of a t-o-t sheet can be seen in Figure 2.17.

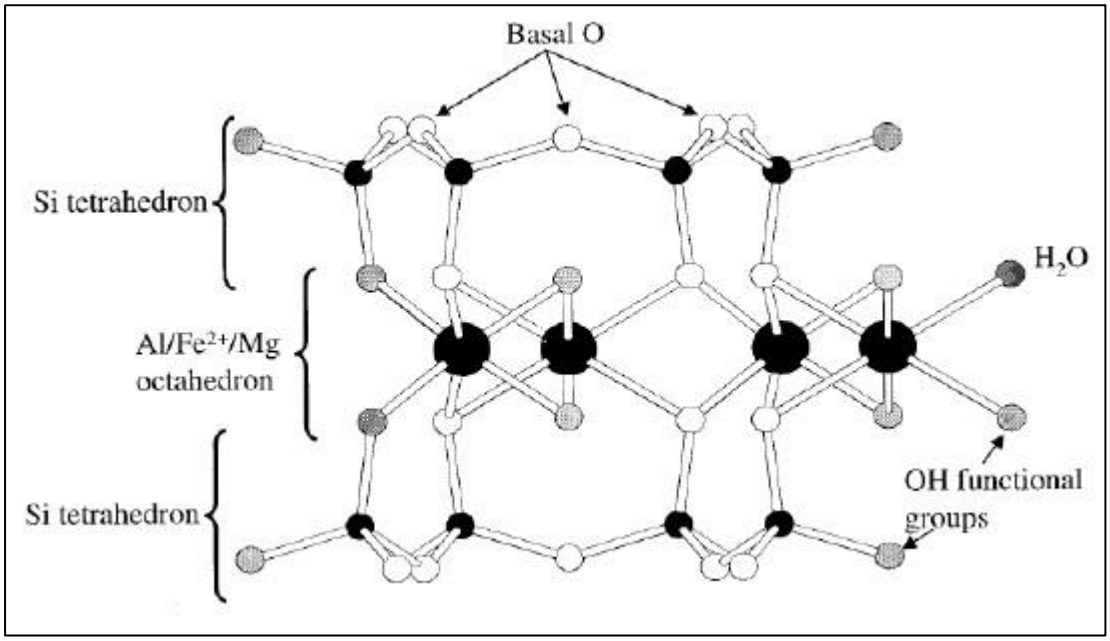

Figure 2.17: Ideal molecular structure of Montmorillonite showing Tetrahedral-Octahedral-Tetrahedral layers (Strawn & Sparks, 1999)

Substitution of the Al^{3+} atoms in the octahedral layer by a cation with a lower valence, such as Mg^{2+} or Fe^{2+}, causes the aluminosilicate sheets to become negatively charged, which is compensated for by exchangeable ions present in the intermediate layer between sheets (Strawn & Sparks, 1999). Water molecules are also able to enter this intermediate layer and cations such as Na^{+}, Mg^{+2} or Ca^{2+} are able to be adsorbed into this layer if encased within a water shell (Van der Wat, 2011). Water molecules and cations which enter the intermediate layer cause inner crystalline swelling to occur. This accounts for the swelling properties of bentonite clay. The swelling causes the surface area of the intermediate layers to increase, leading to a higher cation exchange capacity (CEC). CEC refers to the montmorillonite's capacity to attract cations and is a measure of the clay particle's net negative charge (Vermeulen, 2012)

The edges of the aluminosilicate sheets, while having a smaller surface area, also carry a charge which can be either negative or positive depending on the functional group of the octahedral layer. This allows for anions and cations to be adsorbed onto the edges as well (Vermeulen, 2012). Figure 2.18 shows two montmorillonite t-o-t sheets with interlayer cations and water molecules between them. Due to the fact that the exact elements and ratios of cations within the montmorillonite structure can vary, the chemical formula of montmorillonite is idealised as $(Na,Ca)_{0.3}(Al,Mg)_2Si_4O_{10}(OH)_2.nH_2O$ (Vermeulen, 2012).

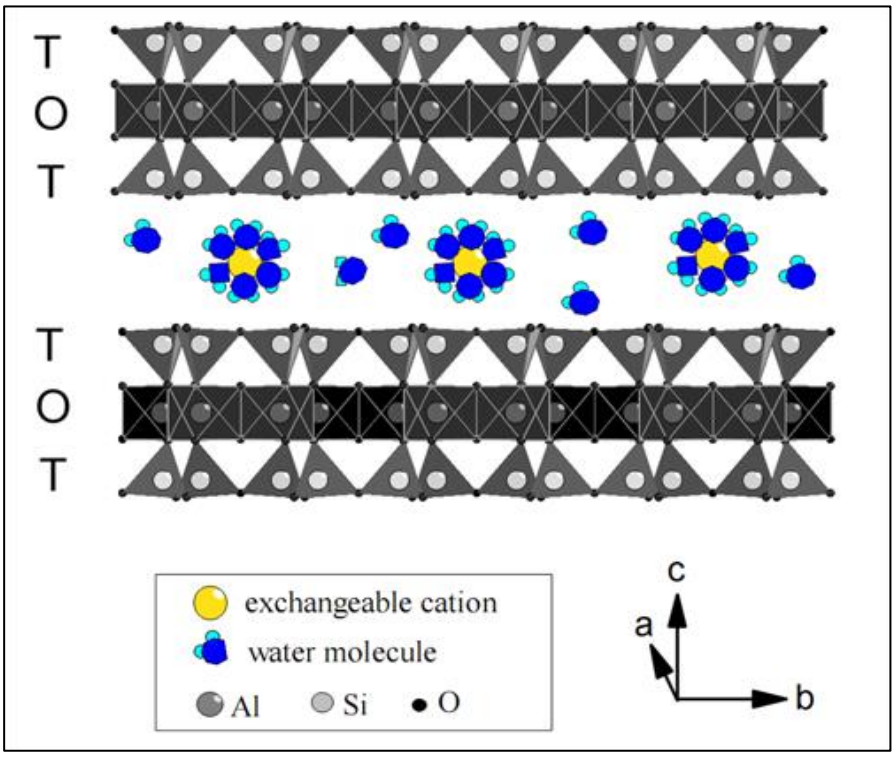

Figure 2.18: Montmorillonite t-o-t sheets with exchangeable cations and water molecules within the intermediate layer (Vermeulen, 2012)

2.4.2 Sorption characteristics of bentonite

Sorption can refer to one of two processes whereby a substance is held or taken up by another substance, namely absorption or adsorption. To prevent confusion both processes will be discussed.

Absorption involves a substance, the absorbate, being taken up into the physical structure of another substance, the absorbent. Absorption normally occurs between substances in different phases, with the absorbent being either a solid, liquid or gas and the absorbate being an ion, molecule or atom. There are a number of requisites in order for absorption to occur. Firstly, the absorbent needs to have a structure which is porous and large enough to accommodate the absorbate. Secondly, the absorbate needs to be a suitable size to fit into the structure of the absorbate. Lastly, an attractive force needs to exist between the two substances in order for absorption to be facilitated (Chromatography Today, 2014).

Adsorption involves one substance or energy, the adsorbate, being attracted to the surface of another substance, the adsorbent, by an attracting force. Two types of adsorption exist, namely chemical adsorption and physical adsorption. In chemical adsorption, also known as chemisorption, an attraction is created due to a chemical reaction which takes place between the adsorbent and adsorbate, while in physical adsorption, attracting forces exist due to weak van der Waals forces (Chromatography Today, 2014).

In the case of bentonite, metal species are adsorbed onto the clay through physical adsorption (Brink, 2012). This adsorption can occur by way of either complex formation (also known as outer sphere adsorption) or ion exchange (also called inner sphere adsorption). Outer sphere adsorption mainly takes place in the interlayer region of the montmorillonite structure, on the basal planes (Indicated on Figure 2.17), by means of electrostatic attraction. Inner sphere adsorption occurs at the amphoteric ligand sites, on the edges of the montmorillonite structure, by forming covalent bonds with functional groups, such as the hydroxyl groups (Indicated on Figure 2.10) (Van der Wat, 2011).

2.4.3 Bentonite in South Africa and availability thereof

As mentioned earlier, different types of bentonite exist depending on the main elements present within its structure. Bentonite mined in South Africa is predominantly of the type which contains both calcium and sodium montmorillonites, and is therefore simply named and referred to as bentonite (Nel et al., 2014). Deposits of relatively pure bentonite in South Africa have been found in the Free State near the town of Koppies, and in the Western Cape

in the Plettenberg Bay district and Heidelberg. Deposits are also found in the Eastern Cape near Jamestown and in Northern Kwazulu Natal at Mkuze. However, these deposits are impure (Agnello, 2005).

Agnello (2005) estimated that bentonite reserves from these deposits are enough to allow production of bentonite to continue at 120 000 tons a year for up to 67 years. Even if production were to increase, the reserves would still last near 50 years if mined at 140 000 tons a year. With the discovery of new bentonite reserves, production of bentonite in South Africa could potentially be prolonged even further (Agnello, 2005).

The bentonite used during the experimental portion of this project was mined from a deposit roughly 30km west of the town of Koppies in the Free State. Mining rights to this deposit is owned by Yellowstar Bentonite, who started mining operations in August of 2011. The quarry stretches over an area of 4 900 square meters and an estimated 27200 tons of bentonite is expected to be recovered from the first 4.5 meters of the deposit (Yellowstar Bentonite, 2015). Waanders (2015) performed X-ray diffraction (XRD) and X-ray fluorescence (XRF) analysis on the clay to determine the mineralogical and chemical compositions thereof. These compositions, as well as physical properties of the clay, are given in Tables 2.1 to 2.4 and Figure 2.19 and 2.20 show photos of the quarry where the clay was mined as well as the on-going excavation operations there.

Table 2.1: Bentonite XRD analyses with values indicating mineral content, with * = smectite type = montmorillonite, ** = illite (Waanders, 2015)

Mineral	Percentage
Clay*	65
Quartz	30
Plagioclase	2
Calcite	<2
Mica**	<2
Kaolinite	<2

Table 2.2: Elemental composition (wt %) of bentonite clay (Waanders, 2015)

Element	Si	Al	Mg	Ca	Na	K	Fe	Ti	C	O
Percentage	24.9	7.6	1.0	1.7	0.5	1.3	6.4	0.4	3.7	52.5

Table 2.3: Compound composition of bentonite clay (Waanders, 2015)

Compound	SiO_2	Al_2O_8	MgO	CaO	Na_2O	K_2O	FeO	TiO_2	CO_2
Percentage	52.3	14.6	1.9	2.7	0.7	1.9	5.1	0.8	20.0

Table 2.4: Bentonite physical properties (Waanders, 2015)

pH (5% in water)	8.4
Moisture (% by weight)	11.5
Viscosity (s)	22.8
Free swell (ml/2g)	10.5
Compactibility (%)	56.5
Base Cation Exchange Capacity (meq/100g)	33.5
Sinter Plate Absorption (%)	370.1

Figure 2.19: Yellowstar bentonite quarry near Koppies, Free State (Yellowstar Bentonite, 2015)

Figure 2.20: Bentonite excavation at Yellowstar bentonite quarry (Yellowstar Bentonite, 2015)

2.5 Heavy metal adsorption model

As previously mentioned, montmorillonite has a permanent surface charge generated in the octahedral layer by replacing Al^{3+} with a lower valence cation, like Mg^{2+}, in the octahedral structure. This charge distributes along the mineral basal planes where it is compensated for and balanced out by the sorption of aqueous cations (such as Mg^{2+}, Ca^{2+}, K^{+} and Na^{+}) into the intermediate layer between t-o-t sheets. Cations in solution can be exchanged with these interlayer cations through outer layer adsorption, by forming surface outer sphere complexes. These exchange reactions are non- specific and occur stoichiometrically (Gu et al., 2010). A variable charge also exists on the edges of the mineral which can be either positive or negative; hence they are called variable edge sites. Adsorption of metal ions to these sites involves the formation of surface inner sphere complexes. These edge sites have a much smaller surface area than the basal planes and therefore accounts for only a small portion of montmorillonite's ion exchange capacity. Montmorillonite has a cation exchange capacity which ranges from 0.7 to 1.3 centi-mol per kilogram (cmol/kg), with only about 20% of this exchange capacity being derived from the variable charges on the mineral's edge (Gu et al., 2010).

Gu *et al*. (2010) and Ikhsan *et al.* (2005) have shown that the adsorption behaviour of metal cations by montmorillonite can be predicted by a 2 site model which uses the two surface sites, the basal surface site ($\equiv X^{-}$) and the edge site ($\equiv SOH$), along with a surface complexation model (SCM). They tested 4 models, namely the Diffuse Layer Model (DLM),

the Triple Layer Model (TLM), the Constant Capacity Model (CCM) and the Extended Constant Capacity Model (ECCM). The DLM model failed to converge, while the TLM and ECCM models had more adsorbing planes and required more fitting data. Since only inner sphere complexation is involved for adsorption on the edge sites, the CCM, which is one of the most widely used SCM's, was chosen. The CCM describes the electrostatic term on the edge site and assumes that all surface complexes are inner sphere surface complexes. The model also assumes that there is a linear relation between the surface charge potential (ψ, measured in J/C) and the surface charge density (σ, measured in C/m^2), shown in Equation 16 (Gu et al., 2010)

$$\sigma = \kappa\psi = T_s F / S_s S_d \qquad \text{(Eq. 16)}$$

Where κ is the capacitance (Farad/m^2), T_s the total surface charge (mol/L), S_s the specific surface (m^2/kg) and S_d the suspension density (kg/L)

The surface reactions and equilibrium constants which were used to complete the model are given by Equations 17 to 21. These equations are for reactions occurring in the presence of a background electrolyte, such as $NaNO_3$.

For the basal surface sites:

$$\equiv X^-.Na^+ + H^+ \rightleftharpoons \equiv X^-.H^+ + Na^+ \qquad \text{(Eq. 17)}$$

$$K_{XNa} = \frac{[\equiv X^- \cdot H^+][Na^+]\gamma_{H^+}}{[\equiv X^- \cdot Na^+][H^+]\gamma_{Na^-}}$$

$$2 \equiv X^- \cdot Na^+ + Me^{2+} \rightleftharpoons \equiv X^- \cdot Me^+ + 2Na^+ \qquad \text{(Eq. 18)}$$

$$K_{XMe} = \frac{[\equiv X_2^- \cdot Me^{2+}][Na^+]^2\gamma_{H^+}^2}{[\equiv X^- \cdot Na^+]^2[H^+]\gamma_{Me^{2+}}}$$

The Na^+ cation in equation 17 and 18 can be replaced by any removable cation such as K^+, Ca^+ an Mg^+, however the Na^+ cation in equation 18 can also be replaced by H^+.

For a positively charged edge site:

$$\equiv SOH^0 + H^+ \rightleftharpoons \equiv SOH_2^+ \qquad \text{(Eq. 19)}$$

$$K_{(+)} = \frac{[\equiv SOH_2^+]}{[\equiv SOH^0][H^+]\gamma_{H^+}} \exp(\psi F / RT)$$

For a negatively charged edge site

$$\equiv SOH^0 + \rightleftharpoons \equiv SO^- + H^+ \quad \text{(Eq. 20)}$$

$$K_{(-)} = \frac{[\equiv SO^-][H^+]\gamma_{H^+}}{[\equiv SOH^0]} \exp(\psi F/RT)$$

For the formation of an inner sphere complex on an edge site

$$\equiv SOH^0 + Me^{2+} \rightleftharpoons \equiv SOMe^+ + H^+ \quad \text{(Eq. 21)}$$

$$K_{SOMe} = \frac{[\equiv SOMe^+][H^+]\gamma_{H^+}}{[\equiv SOH^0][Me^{2+}]\gamma_{Me}^{2+}} \exp(\psi F/RT)$$

Where ≡ is used to indicate a surface site or functional group. ≡X indicates a basal surface site, ≡SOH an edge site, Me a metal ion and square brackets indicate solution concentrations. The exp(ψF/RT) term is used to adjust for the electrostatic properties of the charged surfaces and is derived from the Boltzmann equation, with T being the absolute temperature (298.15K), R the gas constant (8.314 J/mol.K), F the Faraday constant (96 485 C/mol) and ψ the surface potential (Volt). γ is the aqueous activity coefficient calculated from the Davis equation. $K_{(-)}$ and $K_{(+)}$ are the intrinsic proton binding constants and K_{XNa} is the binding constant for the background electrolyte (Gu et al., 2010).

2.5.1 Metal precipitation and co-precipitation

At high pH values it is difficult to distinguish between sorption processes and precipitation reactions. A combination of high pH along with a high adsorbate cation concentration can cause the formation of insoluble metal oxides (Equation 22) or metal hydroxides (Equation 23) which leads to metal precipitation (Bhattacharyya & Gupta, 2008).

$$Me^{2+} + 2H_2O \rightleftharpoons \equiv MeO_{2(s)} + 4H^+ \quad \text{(Eq. 22)}$$

$$Me^{2+} + 2H_2O \rightleftharpoons \equiv Me(OH)_{2(s)} + 2H^+ \quad \text{(Eq. 23)}$$

According to de Pablo *et al.* (2011), precipitation is common with concentrated solutions and cations which form oxides or hydroxides below a pH of 5, such as Cr^{3+}, Cu^{2+} and Pb^{2+}. Adsorption is more likely for cations which precipitate at a higher pH, like Ag^+, Ba^{2+}, Cd^{2+}, Hg^{2+}, Mn^{2+}, Ni^{2+} and Zn^{2+}, or in solutions where ion concentrations are low.

Precipitation of iron onto a surface site causes the formation of large colloidal agglomerates. Other heavy metals in solution, such as nickel, cobalt, manganese and uranium, can

become bound to these agglomerates, leading to the co-precipitation of metals. A model for co-precipitation was developed by Lu *et al*. (2011) with the reactions shows in Equation 24 and 25.

$$\equiv Fe^{s}OH^{0} + Me^{2+} \longrightarrow \equiv Fe^{s}OMe^{+} + H^{+} \quad \text{(Eq. 24)}$$

$$\equiv Fe^{w}OH^{0} + Me^{2+} \longrightarrow \equiv Fe^{w}OMe^{+} + H^{+} \quad \text{(Eq. 25)}$$

In these reactions, s and w are used to indicate a strong or weak site.

2.5.2 Competitive adsorption

When two or more metal species are present in solution, they will compete for the same adsorption sites. Gu *et al.* (2010) investigated the adsorption of five metals onto montmorillonite and found the adsorption affinity of the charged basal planes to be Pb>Cu>Ni≈Cd≈Zn. For the variable charged edge sites the affinity changed to Pb>>Cu>Zn>Cd>Ni. De Pablo *et al.* (2011) reported a selectivity sequence Hg>Cu>Pb>Zn>Cr>Ni>Ag>Ba>Cd>Mn and the sequence observed by Khalili *et al.* (2013) was Th>U>Pb>Cr>Zn>Mn. By adding the work of Vermeulen (2012) an assumed selective adsorption sequence can be formed, with the order: U^{4+}>Cr^{3+}>Al^{3+}>Fe^{3+}>Ca^{2+}>Hg^{2+}>Pb^{2+}>Cu^{2+}>Mg^{2+}>Zn^{2+}>Fe^{2+}>Cd^{2+}≈Ba^{2+}≈Co^{2+}>Ni^{2+}>Mn^{2+}>> NH^{4+}>K^{+}>H^{+}>Na^{+}>Li^{+}

Higher adsorption affinity of metal species can be attributed to higher softness, which is characterised by lower electronegativity, smaller ionic potential and larger ionic radius (Vermeulen, 2012)

2.5.3 Effect of pH

As is evident from previous sections, pH is an important factor which affects the removal of heavy metals from AMD. The adsorption potential of montmorillonite is determined by the activity of H^{+} and OH^{-} ions which react with its surface. At low pH levels, these ions compete with metal cations for binding sites, causing metal adsorption to decrease. With an increase in pH however, more binding sites become available and metal adsorption increases. More sites will become available for metal adsorption as the pH increases further and, once the pH is high enough, metal hydroxides will also form and start to precipitate, increasing the effective removal of heavy metals (Ijagbemi et al., 2010).

2.5.4 Effect of time

Adsorption processes are considered to be very fast physic-chemical reactions. Time dependent adsorption experiments performed by Ijagbemi *et al.* (2010), which focussed on the adsorption of Ni^{2+} onto montmorillonite, showed that the maximum uptake of Ni^{2+} was achieved between 210 and 250 minutes. Xu *et al.* (2008) performed a similar experiment and found that the maximum adsorption occurred after a period of about 120 minutes. The differences in their results could be attributed to pH differences, montmorillonite composition or the ionic concentration of the Ni^{2+}.

Wu *et al.* (2011) studied the adsorption of Cu^{2+}, Cd^{2+} and Cr^{2+} onto montmorillonite and found that after 10 minutes of rapid adsorption, adsorption started to decrease, eventually reaching equilibrium after approximately 60 minutes. During the first 10 minutes, adsorption sites on the montmorillonite were plentiful, allowing for the metal ions to interact with the sites easily, accounting for the rapid adsorption. After this time the sites available for adsorption, as well as the concentrations of the metal ions, began to decrease, causing the adsorption rate to slow until equilibrium was reached (Wu et al., 2011). The results of this experiment are shown in Figure 2.21.

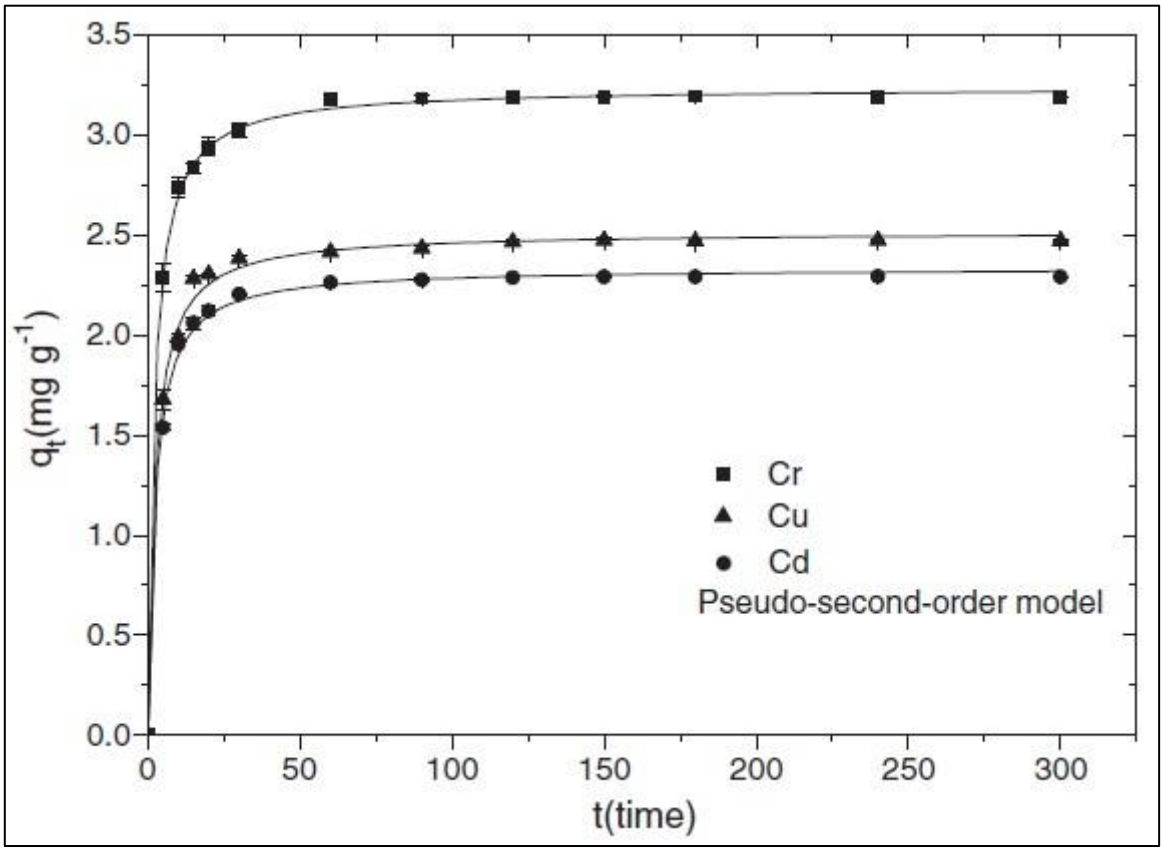

Figure 2.21: Adsorption of Cr^{3+}, Cu^{2+} and Cd^{2+} onto montmorillonite over time. q_t is the adsorbed amount at a specific time, t. Taken from Wu *et al.* (2011)

2.5.5 Stirring versus shaking

Ntwampe *et al.* (2015) used bentonite clay along with $Ca(OH)_2$, $Mg(OH)_2$ and slaked dolime to test whether the agitation method used to mix these compounds into the AMD for treatment had any effect on the amounts of suspended contaminants removed from it. Solids in suspension increase the turbidity of a liquid, giving it a cloudy or hazy appearance. As mentioned earlier, solute ions can be removed from the AMD by forming solid compounds which can precipitate. For suspended solids to be removed however, coagulation and flocculation needs to occur before they can settle. Agitation through stirring or shaking is essential during AMD treatment as it induces a velocity gradient which disperses the reagents throughout the solution. The type of coagulant which is used and the length of time that mixing occurs determines the optimum velocity gradient. During mixing, physico-chemical reactions take place in the system, causing destabilization, hydrolysis and aggregation to occur. These reactions take place during the coagulation and flocculation stages which occur during rapid mixing and slow mixing respectively. During coagulation, small primary flocs are formed which enlarge during flocculation into secondary larger flocs (Ntwampe et al., 2015).

Mixing speed is very important as it influences the rate at which flocs can collide to form secondary larger flocs, but the shear stresses from mixing can also rupture the flocs, causing them to re-stabilize and stay suspended. The experiments conducted by Ntwampe *et al.* (2015) used both stirring and shaking to mix the AMD samples at 250 rpm for 2 minutes. Three pH adjuster compounds were used, calcium hydroxide, magnesium hydroxide and slaked dolime, and for each compound a stirring and shaking test was performed. Turbidity was measured before and after treatment to determine the removal of colloidal particles from the AMD samples. The AMD had an initial turbidity of 100 NTU (Nephelometric Turbidity Units). The results (Figure 2.22) however showed that there was no significant difference in the turbidity removal between the samples which had been stirred and those that had been shaken.

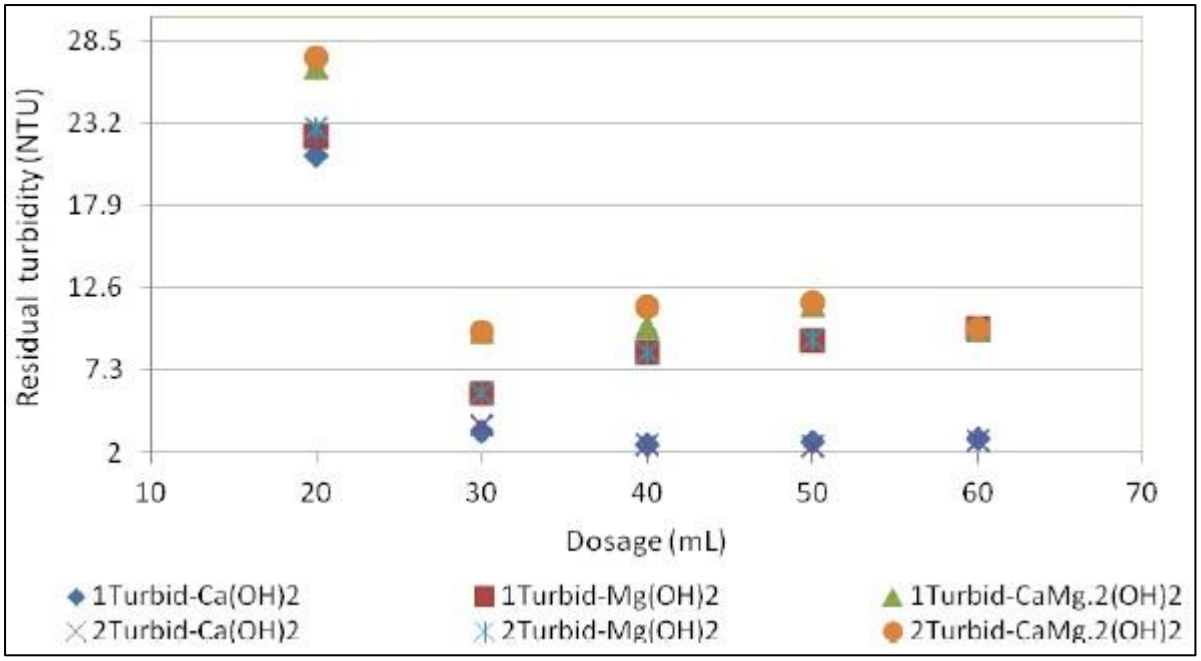

Figure 2.22: Residual turbidity graph of AMD treated with $Ca(OH)_2$, $Mg(OH)_2$ and slaked dolime comparing mixing via shaking and stirring. (♦= $Ca(OH)_2$ + stirring, ■=$Mg(OH)_2$ + stirring, ▲= $CaMg.2(OH)_2$, x= $Ca(OH)_2$ + shaking, ж= $Mg(OH)_2$ + shaking, ●= $CaMg.2(OH)_2$ + shaking) (Ntwampe et al., 2015).

2.6 Dolomite rock

Dolomite rock, sometimes referred to as dolostone, is a sedimentary rock which primarily consists of a mineral called dolomite, which is a double carbonate of calcium and magnesium ($CaMg(CO_3)_2$). Dolomite is formed due to the chemical alteration of limestone deposits by groundwater with high magnesium concentrations. Because of this, dolomite is very similar to limestone, having nearly the same hardness, white-grey/brown colour and acid neutralisation abilities (King, 2015).

Theoretically dolomite is made up of almost equal parts $CaCO_3$ (54.35%) and $MgCO_3$ (45.65%), however considerable variations can occur in nature. The mineral is referred to as calcitic- or lime dolomite in instances where the $CaCO_3$ content is more than 10% higher than the theoretical composition, while dolomite with an increased $MgCO_3$ content of between 5% and 10% is called magnesia limestone. For all intents and purposes, dolomite with a $MgCO_3$ content of less than 5% is generally taken to be normal limestone (Minerals Zone, 2014). It is normal for dolomite to contain certain impurities such as iron oxide, silica and alumina, though the combined percentage of these impurities is usually low and not higher than 7% (Minerals Zone, 2014).

As with limestone and burnt lime, calcined/burnt dolomite is more effective for AMD treatment than normal dolomite. Burnt dolomite is referred to as dolime, and is formed by

the same process as lime, by heating dolomite to 900°C or above causing carbon dioxide to be released, leaving calcium magnesium oxide according to Equation 26 (Ispat Digest, 2014). Figure 2.23 shows the different appearance of dolomite and dolomite which has been burnt to form dolime.

$$CaCO_3 \cdot MgCO_3 + Heat \rightarrow CaO \cdot MgO + 2CO_2 \quad \text{(Eq. 26)}$$

Figure 2.23: Visual comparison of dolomite (Right) and dolime (Left) (Lhoist, 2015)

As with lime, dolime can also be slaked with water to convert the calcium oxide and magnesium oxide to their hydroxide forms for more effective AMD treatment, as shown by Equation 27.

$$CaO \cdot MgO + 2H_2O \rightarrow Ca(OH)_2 \cdot Mg(OH)_2 \quad \text{(Eq. 27)}$$

Because slaked dolime also contains calcium hydroxide, like slaked lime, $CaSO_4$ will form when it is used to treat AMD with high sulphate levels (Brink, 2012). However, as stated in section 2.3, it is possible to precipitate this $CaSO_4$ from the water by the addition of magnesium compounds. Because dolime contains both calcium and magnesium hydroxide, it may be possible that the calcium sulphate can be precipitated from the water without the addition of extra magnesium compounds, instead relying on the magnesium hydroxide already present.

Chapter 3 : Experimental

In Chapter 3 the experimental part of the project will be discussed. Chemicals which were used, the steps followed during the experiments as well as any preparation done beforehand will be discussed.

3.1 Chemicals and their preparation

Before the start of the experimental runs certain chemicals and compounds needed to be acquired and prepared for the experimental work. Here follows a list of the chemicals used during the experimental procedure as well as the methods by which they were prepared.

3.1.1 Acid Mine Drainage/Water (AMD/W)

A 25 litre AMD sample was collected from the Harmony Gold mining company's Tweelopiespruit AMD treatment site near Krugersdorp at coordinates 26°06'55.1"S 27°43'22.2"E. This sample was left for a period of 1 month to allow for oxidation and acidification to occur. At the start of the first and second experimental run the AMD sample was at a pH level of roughly 1.97. After the completion of the first and second set of experimental runs, a second AMD sample was acquired from the same source as the first and was again left to oxidise and acidify. The pH level of the second sample was approximately 2.53 when the third and fourth sets of experiments were started. ICP analysis was performed on both samples to determine the concentrations of contaminants which were present in the water. Table A.1 and A.2 in Appendix A shows the results of these analyses.

3.2.2 Bentonite clay

Bentonite clay was obtained from the Yellowstar Bentonite mine, a bentonite mining and supplying company situated in Parys in the Free State. The bentonite used was mined from a quarry located at coordinates 27°16'40.2"S 27°15'06.5"E, near the town Koppies. Specifications for the bentonite can be found in Tables 2.1 to 2.4 in section 2.4.3. The as received clay contained lumps varying in size from ≈5mm to about the size of a golf ball (Figure 3.1) and was placed in a ball mill for an hour to grind it into a fine powder (Figure 3.2). This was done in order to make the clay's handling easier and to increase the active surface area available for adsorption. Before each experimental run the clay was prepared

by adding it to deionised water at a ratio of 5g clay to 200ml water to create a clay suspension.

Figure 3.1: Bentonite clay as it was received from Yellowstar Bentonite

Figure 3.2 Bentonite clay powder after grinding in a ball mill

3.1.3 Burnt dolomite

Dolomite rock was acquired from a field at coordinates 25°50'58"S 27°59'46"E. This dolomite falls under the Malmani dolomites, a subgroup of the Transvaal Supergroup, which is a geological sedimentary rock sequence occurring in many locations in South Africa. According to Brink (2012), an analysis done by Du Toit in 1954 on Malmani dolomite showed a composition of 48.4% $CaCO_3$ and 40.6% $MgCO_3$, with the remainder made up of traces of $FeCO_3$, $MnCO_3$ and silicate. XRF analysis of the dolomite used for this project indicated a composition of 54.2% $CaCO_3$ and 45.8% $MgCO_3$. The dolomite rock was dug out as hand sized chunks (Figure 3.3) and crushed using a jaw crusher. The size was gradually reduced by multiple passes through the crusher till pieces of roughly 1-2 cm were acquired. A rotary impact mill was then used to further reduce the particle size between 1 and 5 mm, however this size was still too large for use in the laboratory. A final size reduction was done by placing the particles into a ball mill for about an hour until it became a fine powder which was then placed into an electric oven at a temperature of 1000°C for a period of 1 hour till the powder attained a visible light orange-brown colour. After cooling down, the calcined dolomite powder (Figure 3.4) was ready for use. Since this powder consists roughly of 50% calcium oxide (CaO) and 50% magnesium oxide (MgO) the general chemical formula $CaMgO_2$ is used for it. For experimental use, 20g of the dolime powder was slaked with 200ml deionised water, creating a 10% calcium magnesium hydroxide ($Ca(OH)_2.Mg(OH)_2$) solution. As mentioned before, dolime was chosen for the pH adjustment to test whether the use thereof could negate lime scaling, which forms when using pure lime for pH adjustment.

Figure 3.3: Dolomite rock before crushing

Figure 3.4: Dolime powder formed by crushing and burning dolomite

3.1.4 Calcium hydroxide ($Ca(OH)_2$)

The Calcium hydroxide which was used was procured from Associated Chemical Enterprises (ACE Chemicals). This chemical is graded as a platinum line chemical, meaning it is of an analytically pure quality. This chemical was made up to a 0.5% solution for experimental use, using 500ml deionised water and 2.5g $Ca(OH)_2$.

3.1.5 Magnesium hydroxide ($Mg(OH)_2$)

The Magnesium hydroxide used was also supplied by ACE Chemicals and had a gold line chemical grade, thus a chemically pure quality. As with the other chemicals, 500ml deionised water was added to 2g $Mg(OH)_2$ to make a 0.4% solution for use during the experimental runs. Calcium hydroxide and Magnesium Hydroxide were tested separately in order to compare their effectiveness with that of the burnt dolomite, which contains both of these compounds.

3.2 Experimental procedure

The experimental work done for this project consisted of three separate experimental runs, with each run being made up of 4 to 6 separate tests. Before each experimental run, pH calibration curves were also set up for each individual pH adjustment solution. Here follows the steps and procedures which were followed before and during the experiments.

3.2.1 pH calibration curves

Before the start of each experimental run, pH calibration curves were set up for each individual pH adjusting solution which was to be used, namely the $Ca(OH)_2.Mg(OH)_2$ solution prepared from the burnt dolomite, and the pure $Ca(OH)_2$ and $Mg(OH)_2$ solutions. For each calibration curve 300ml of the AMD sample was placed into a 600ml glass beaker and its pH measured. The base solution was added to the sample incrementally and the mixture was stirred for 10 minutes after each addition. Once stirring was complete the mixture was left to stand for another 10 minutes, after which the pH was measured and recorded. This was repeated until enough data points had been recorded to construct a representative pH curve for the base solution. Three calibration curves were constructed in total.

3.2.2 First experimental run

For the first experimental run, 900ml of the AMD water sample was removed from the sample container and evenly divided into 3 separate 600ml glass beakers. An amount of the $Ca(OH)_2.Mg(OH)_2$ solution was added to each to adjust the pH level. The samples were stirred for 5 minutes via a mechanical stirrer (Figure 3.5) and allowed to stand for another 10 minutes before the pH was tested. If the pH was not within the correct pH range, another dose of Calcium Magnesium Hydroxide solution was added and the process repeated until the correct level was obtained. Once the pH was correct, 50ml of the bentonite clay suspension was added to each beaker and the beakers were placed back into the mechanical stirrer. The samples were each stirred for 2 minutes at a speed of 250rpm (rapid mixing) after which the speed was slowed to 130rpm and stirring continued for another 10minutes (slow mixing). After stirring, the samples were removed from the stirrer and left to stand for a period of 1 hour to allow settling to occur. The stirring time, speed and settling time was chosen based on the work done by Ntwampe *et al.* (2015). A 50ml sample of the clear supernatant was recovered from each beaker and kept for further ICP analysis. This process was repeated for each pH range which was to be tested, starting at a pH range of 6

to 7 and ending at a pH between 11 and 12. A pH range higher than 11-12 was not tested as the highest pH which could be obtained by adding $Ca(OH)_2.Mg(OH)_2$ was 11.42. A total of 6 runs were done and 18 supernatant samples were recovered.

Figure 3.5 Mechanical stirrer used for mixing of AMD samples

3.2.3 Second experimental run

The second experimental run was performed in the same manner as the first. During this run however, pure $Ca(OH)_2$ solution was used for pH adjustment instead of the calcium magnesium hydroxide solution. The pH ranges for this run started at pH between 6 and 7 and ended at 9-10. The highest pH which could be reached by adding $Ca(OH)_2$ was 9.4 and thus a higher pH range was not tested. In total 4 runs were completed and 12 supernatant samples were recovered

3.2.4 Third experimental run

The third experimental run was performed exactly as the second but used pure $Mg(OH)_2$ solution for pH adjustment. The highest pH which could be obtained using the $Mg(OH)_2$ was 9.13, therefore the pH ranges which were tested also ended at range 9-10.

3.2.5 ICP-OES analysis

An Agilent Technologies 700 Series ICP-OES (Figure 3.6) was used to determine the concentrations, measured in parts per million (PPM), of contaminant elements in the AMD samples and the treated supernatant samples. Before the samples could be analysed with the ICP-OES apparatus, the samples first had to be prepared. A 1% nitric acid (HNO_3) solution was made by making up 10ml of acid to 1litre with deionised water. 20ml of the acid solution was added to 2ml of each of the supernatant samples in a test tube for a dilution factor of 11. The test tubes with the diluted samples were then loaded into a tube tray before being placed into the ICP-OES machine for analysis.

Figure 3.6: Agilent Technologies 700 Series ICP-OES

Inductively coupled plasma optical emission spectrometry (ICP-OES) is one of the most powerful analytical techniques used for the determination of trace elements in a myriad of sample types. The ICP was developed specifically for OES in the mid-1960s at Iowa State University, and in 1974 the first commercial ICP-OES instrument was introduced. Since it was developed, the ICP has become the most popular source for OES, and it is also used for inductively coupled plasma mass spectrometry (ICP-MS) as an ion source. Over the past 35 years, elemental detectability for ICP-based spectroscopic techniques have been continuously and dramatically improved, with the detection limits for many elements increasing by factors of four to six orders. ICP-OES combines a wavelength selection

device and a photodetector with a high temperature ICP source to identify and determine the concentration of elements within a sample (Hou & Jones, 2000).

The plasma which is used for ionisation is formed in a stream of argon gas which flows through an assembly of 3 concentric quartz tubes at 8-20 L/min. This assembly, known as a plasma torch, generally has an internal diameter of 18mm. A copper induction coil (also known as the load coil) which is connected to a radiofrequency (RF) generator encircles the top of the plasma torch and is cooled by either water or by the argon gas (Montaser, 1998). The RF generator, operating at a frequency of 27 – 40 MHz and an output of 1-2kW, generates a magnetic field through the load coil, which induces a current in the argon gas stream (Montaser, 1998). When a spark is applied to the argon gas stream, the argon atoms have their electrons stripped off and ions are formed. These ions are caught within the oscillating magnetic field and collide with other argon atoms to form an argon plasma discharge (Wolf, 2005) This plasma, with a temperature of about 6000-10000 K, is stable and self-sustaining for as long as the gas continues to flow in a symmetrical pattern and the magnetic field strength remains sufficiently high (Montaser, 1998).

Typically, the sample which is being tested is aerosolised before being introduced into the plasma. This can be done by using a laser to convert solid samples directly into an aerosol or by aspirating a liquid or dissolved solid sample into a nebulizer. The elements within the sample aerosol are quickly vaporized upon entering the plasma and are liberated as free atoms. Within the plasma, the atoms collide, imparting additional energy to them and promoting them to excited states. Ions are also often formed if enough energy is available and enter an excited state as well. Figure 3.7 shows a schematic drawing of an ICP torch.

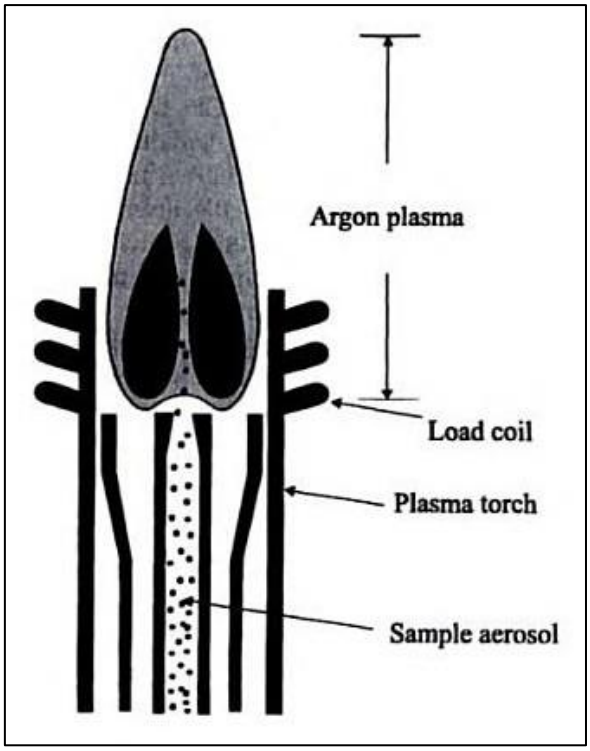

Figure 3.7: Schematic of an ICP torch viewed side-on (Montaser, 1998)

Through the emission of a photon the atomic and ionic excited state species are able to return to the ground state. Photons have distinguishing energies which are determined by the quantized energy level structure of the ions or atoms that released them, meaning the elements which they originated from can be identified by the photons' wavelengths. The total number of photons and the concentration of the originating element in the sample are directly proportional to one another. Thus, the higher the concentration of an element in the sample is, the higher the number of photons for that element will be (Hou & Jones, 2000).

A concave mirror or a lens is used to collect and focus a portion of the photons emitted from the ICP onto the entrance aperture of a wavelength selection device, such as a monochromator. A photodetector then converts the wavelength which exits the wavelength selection device into an electrical signal which is amplified and processed by the detector electronics to identify the sample element (Hou & Jones, 2000).

Chapter 4 : Results and discussion

In this chapter the results that were obtained from the ICP-OES analysis performed on the supernatant collected during each of the three experimental runs, which were performed to study the effectiveness of bentonite clay adsorption on the treatment of AMD with pH adjustment will be discussed. While only some results will be discussed here, all of the ICP-OES analysis results can be found in Appendices B to D.

4.1 pH calibration curves

The calibration curves (Figure 4.1, 4.2 and 4.3) were produced by adjusting the pH of an AMD sample, in order to know the amounts of $Ca(OH)_2.Mg(OH)_2$. $Ca(OH)_2$ and $Mg(OH)_2$ required to achieve a certain pH value. The pH and dosage values from these graphs were used to prepare AMD samples with the desired pH values for use during the experimental runs.

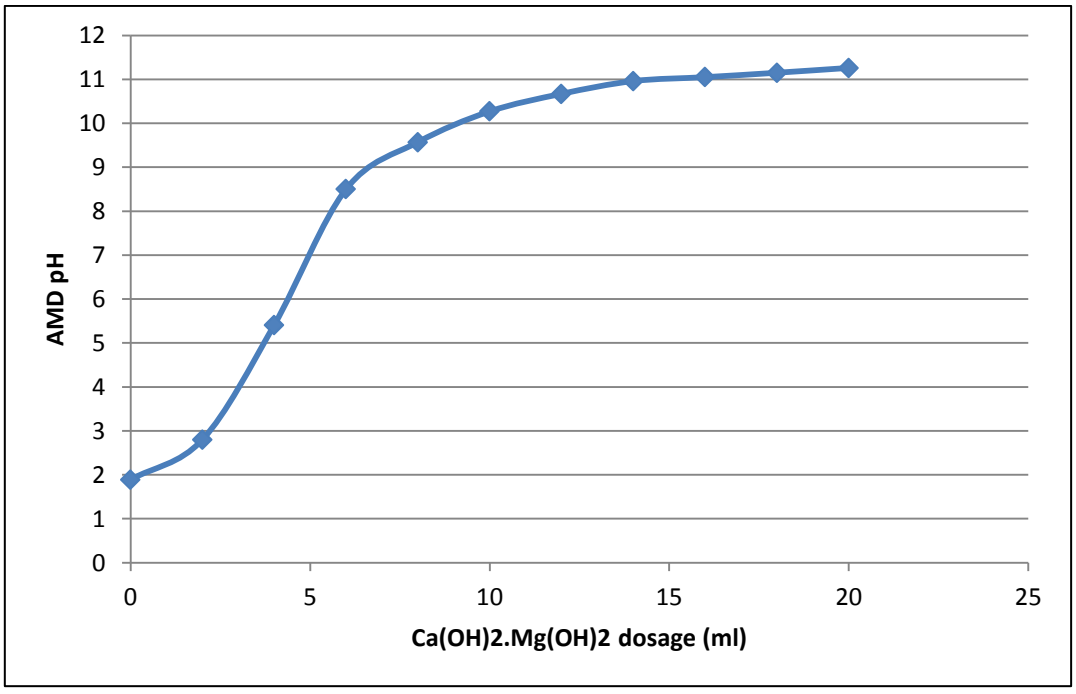

Figure 4.1 pH calibration curve for hydrated dolime

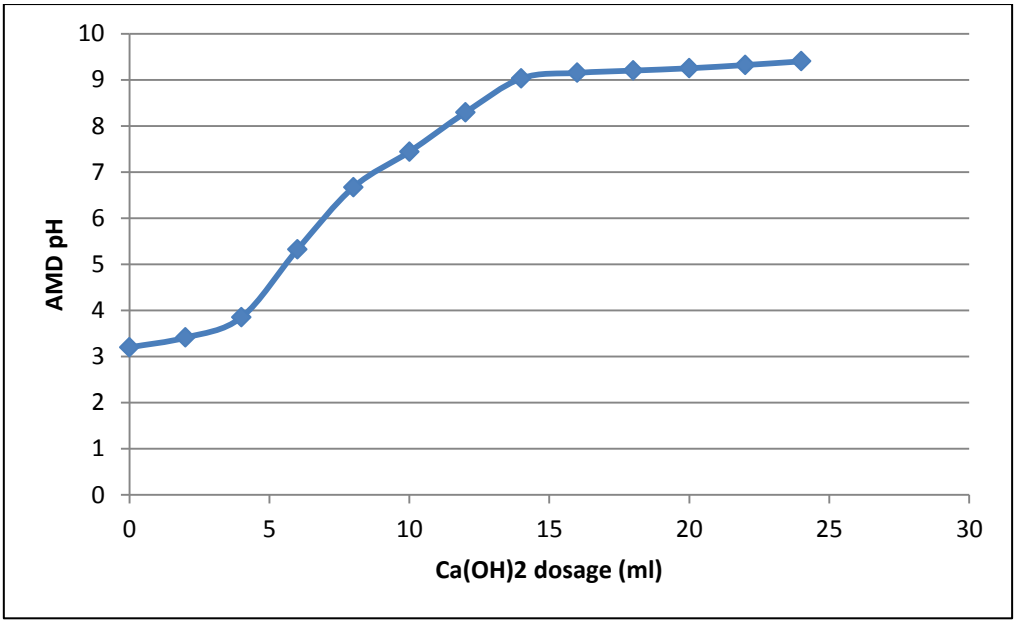

Figure 4.2: pH calibration curve for calcium hydroxide

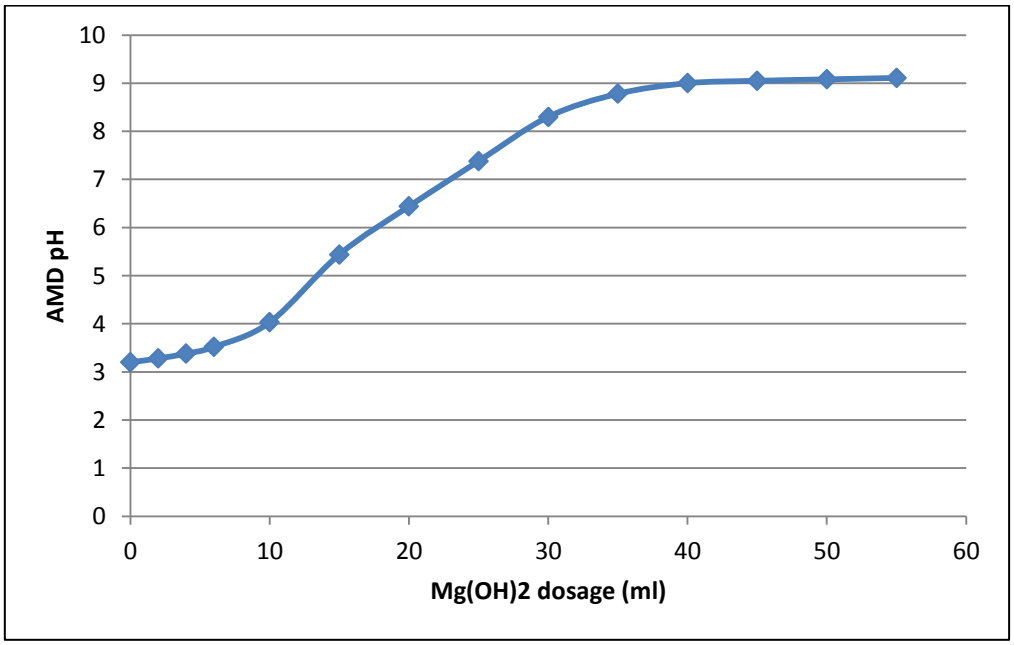

Figure 4.3: pH calibration curve for magnesium hydroxide

4.2 First experimental run

In the first experimental run slaked dolime ($Ca(OH)_2.Mg(OH)_2$) was used to adjust the pH of the AMD sample in an effort to determine if the magnesium content thereof would solve the problem of gypsum formation. The first indication that the treatment had been successful in cleaning the AMD could be seen in the appearance of the recovered supernatant samples.

It was apparent once treatment was complete that the supernatant was much clearer than the original raw AMD (Figure 4.4). This coincides with the work done by Ntwampe *et al.* (2015) who used bentonite clay along with $Ca(OH)_2$, $Mg(OH)_2$ and slaked dolime to decrease the turbidity of AMD.

Figure 4.4: Visual comparison of raw AMD (left) and supernatant (right) recovered from AMD treated with slaked dolime and bentonite clay

Figure 4.5 shows the concentrations of the 4 elements of most concern within the AMD for the project, namely Fe, Ca, Mg and S, after pH adjustment and bentonite clay treatment. It must be noted that the concentrations shown at pH 1.97 are the concentrations present in the raw AMD sample before treatment. Also, although the results show the concentration of elemental sulphur within the AMD, it is believed that most of the concentration of sulphur in the solution appears as sulphate ions (SO_4^{2-}), this is based on the stoichiometric mole ratio of 1 to 1.

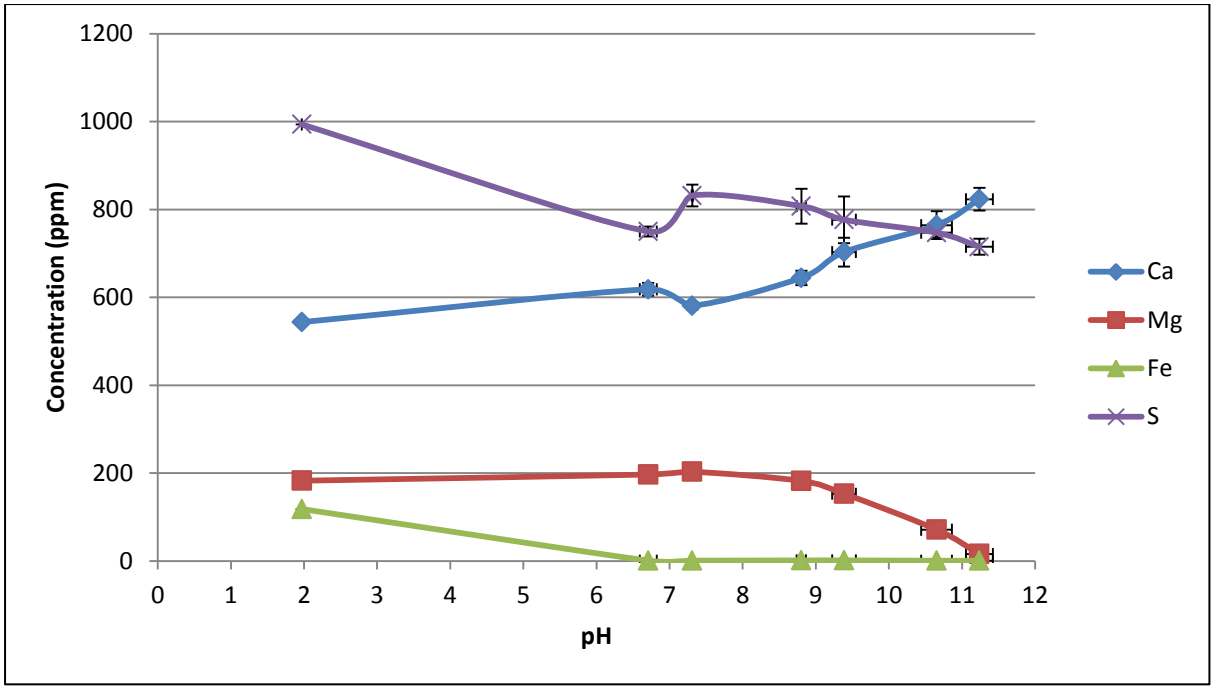

Figure 4.5: Concentrations of Ca, Mg, Fe and S* in AMD after treatment with bentonite clay at different pH levels (pH adjusted by addition of slaked dolime) *S = SO_4^{2-}

It is observed (Figure 4.5) that the treatment method was successful in removing nearly all traces of iron from the AMD, even at the lowest pH range (pH = 6-7). This is in agreement with the literature (Figure 2.5) that Fe^{3+} readily precipitates as ferric hydroxide at pH levels around 3.5, owing to the red-orange colour of the AMD. Increasing the pH resulted in the precipitation of nearly all the Fe in solution, subsequently causing it to be adsorbed onto the surface of the added bentonite clay. As nearly all traces of iron was removed from the AMD at pH 6.7, it can be assumed that all of the iron in solution was fully oxidised Fe^{3+} ions, as Fe^{2+} ions only starts to precipitate as ferrous hydroxide around pH 7-8 (Figure 2.5).

The concentration curves of Mg^{2+} and Ca^{2+} (Figure 4.5) indicate that the $Mg(OH)_2$ present in the slaked dolime could not prevent the formation of aqueous gypsum, nor was it able to cause it to precipitate. This assumption is based on the increasing concentration of calcium in solution whereas the concentration of the magnesium in solution decreased. If the $Mg(OH)_2$ had been successful in causing the gypsum to precipitate, both calcium and sulphate concentrations would have decreased while the concentration of magnesium in solution rose. According to literature (Aubé, 2004) it is known that the formation of gypsum is very slow in comparison with metals precipitation, and it is also stated that magnesium enters its active region at pH 8-12 (Metcalf & Eddy, 2003). It is speculated that once the active pH level of magnesium is reached it precipitates as $Mg(OH)_2$ before the formation of gypsum occurs, i.e. by the time aqueous gypsum is formed there is no magnesium left in solution to precipitate it.

According to Figure 4.5, there was an almost 250 ppm decrease in the concentration of sulphate ions after treatment at pH 6.7, which can be attributed to bentonite adsorption. Beyond pH 7.3 the sulphate levels decrease once again, inevitably due to bentonite adsorption, however, there is a possibility that some of the sulphate ions precipitated with Ca^{2+} as gypsum between pH 7.3 and 11.2. If this is true, the amount of sulphate which precipitates as gypsum should be rather minute as it can be seen that the concentration of calcium in solution is rising steadily between these pH levels. This means that, if gypsum precipitation is indeed occurring, not enough of it is precipitated to impact the concentration of Ca^{2+} in the solution in any significant way. The rise in Ca^{2+} ions in the solution is due to the constant addition of $Ca(OH)_2$ with slaked dolime for pH adjustment. The sudden rise and drop of the concentrations of sulphate and calcium respectively between pH 6.7 and 7.9 is believed to be attributed to the transition phase of the AMD from acidic to basic at pH 7. At neutral pH, there is less reactivity due to the equilibrium state between the van der Waals forces of attraction and the electrostatic forces of repulsion (Gregory & Duan, 2001), a condition which is also applicable to the cations and anions.

4.3 Second experimental run

In the second experimental run pure analytical grade $Ca(OH)_2$ was used for pH adjustment, representing the common method of treating AMD with hydrated lime, but with the addition of bentonite clay.

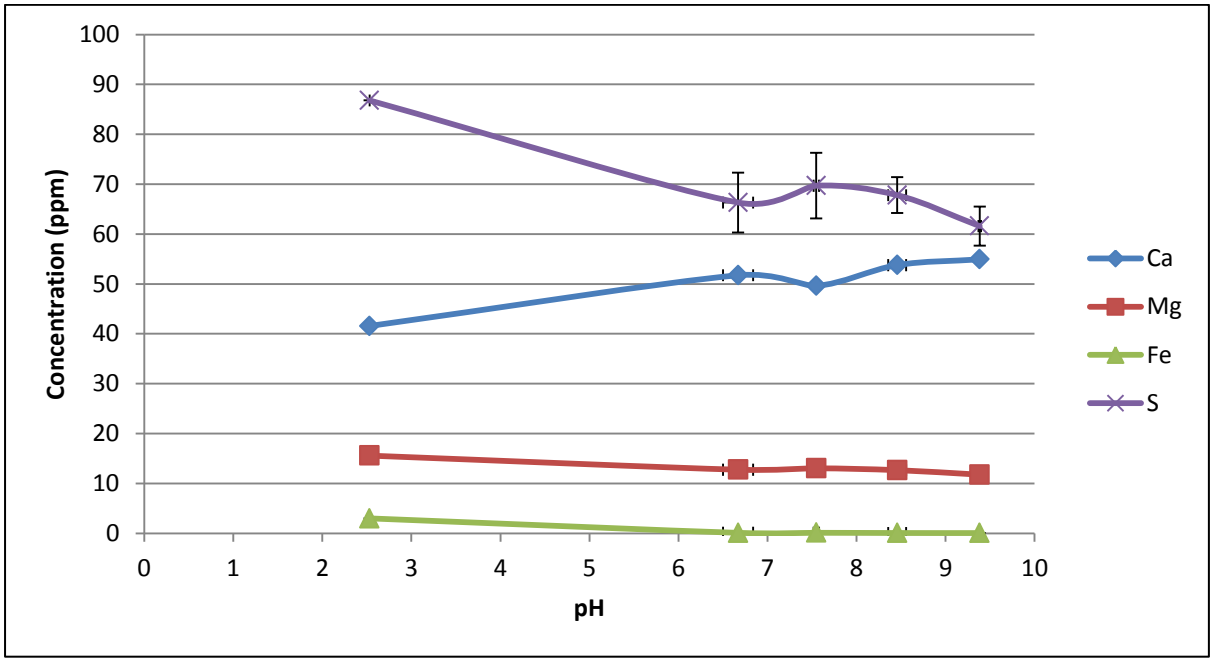

Figure 4.6: Concentrations of Ca, Mg, Fe and S* in AMD after treatment with bentonite clay at different pH levels (pH adjusted by addition of calcium hydroxide) *S = SO_4^{2-}

It is apparent from Figure 4.6 that that the initial concentrations of Ca, Mg, Fe and SO_4^{2-} in the raw AMD are relatively lower than in the AMD sample used during the first experimental run. The sulphate levels are lower by roughly 900 ppm, calcium by 500 ppm and magnesium is almost 170 ppm less than in the first AMD sample, with iron being almost non-existent at only 3 ppm. As mentioned in section 2.1.6, the AMD treatment site where both the first and second samples were collected from, belonging to Harmony Gold Mining Company, changed their AMD treatment process within the last 2-3 years. A recycle step was added to the treatment process to recycle part of the treated and neutralised AMD back into the mine void where the raw AMD is generated from. It is believed that this recycled neutralised AMD, which contains hydrated lime and limestone, may be slightly increasing the pH of the raw AMD contained within the mine void. The pH of the first AMD sample was 1.97 while that of the second sample was 2.53. While this may not seem like a significant change, remember that AMD discharges from this mine at 15-20 million litres per day, not accounting for the AMD still contained within the mine. Changing the pH of such a large volume of liquid, even in the slightest, is no small feat. It is possible that this small rise in pH may be causing contaminants in the raw AMD to precipitate within the mine, leading to lower concentrations of these contaminants in the AMD which is discharged from the mine. The difference between the two AMD samples used in this study is visually apparent as well, with the first sample having a deep orange-red colour to it while the second sample appears much clearer (Figure 4.7).

Figure 4.7: Visual comparison of the first (left) and second (right) AMD samples collected from the Harmony AMD treatment site

Despite the low contaminant concentrations within the second AMD sample, it is observed from Figure 4.6 that after treatment at pH 6.7, 7.5, 8.5 and 9.4, the Ca and S curves follow the same trend as was seen in the results for the first experimental run (Figure 4.5). This could further support the statement that magnesium did not influence the precipitation of gypsum in the previous experiment, since the addition of $Mg(OH)_2$ in that experiment yielded a similar sulphate and calcium curve as this experiment where no $Mg(OH)_2$ was added. As before, the decreasing sulphate concentration between the pH of 2.53 and 6.7 can be attributed to bentonite adsorption, while adsorption and precipitation play a role above the pH of 7.5. The concentration of Ca in solution increased because of the addition of $Ca(OH)_2$ to the AMD sample to increase the pH. Above pH 7.5 the active region of calcium is reached and it starts to react with SO_4^{2-} ions to form aqueous gypsum. It is interesting to note that 2 days after the completion of the second experimental run, white rings started to form on the inside of some of the glass beakers which were used during the experiments. Washing with water did not remove these rings and hydrochloric acid (HCl) needed to be used. It is very possible that these rings were gypsum scaling which was not removed or noticed during the initial cleaning of the beakers after the second experimental run had ended.

Based on magnesium's initial (15.6 ppm) and final (9.4 ppm) concentrations, no significant reactions for this element occurred. The initial iron concentration in the AMD was extremely low, only 3 ppm. The final value shows that the concentration did decrease to ≈0.06 ppm, though at such a low concentration and such a small difference between the initial and final value, it is hard to say whether the decrease is due to bentonite adsorption or simply human or equipment error.

4.4 Third experimental run

Chemically pure $Mg(OH)_2$ was used to control the pH level of the AMD samples of the third experimental run to determine its effect on the removal of Ca ions already in the AMD, based on the study done by Brink (2012). Figure 4.8 shows the results which were obtained.

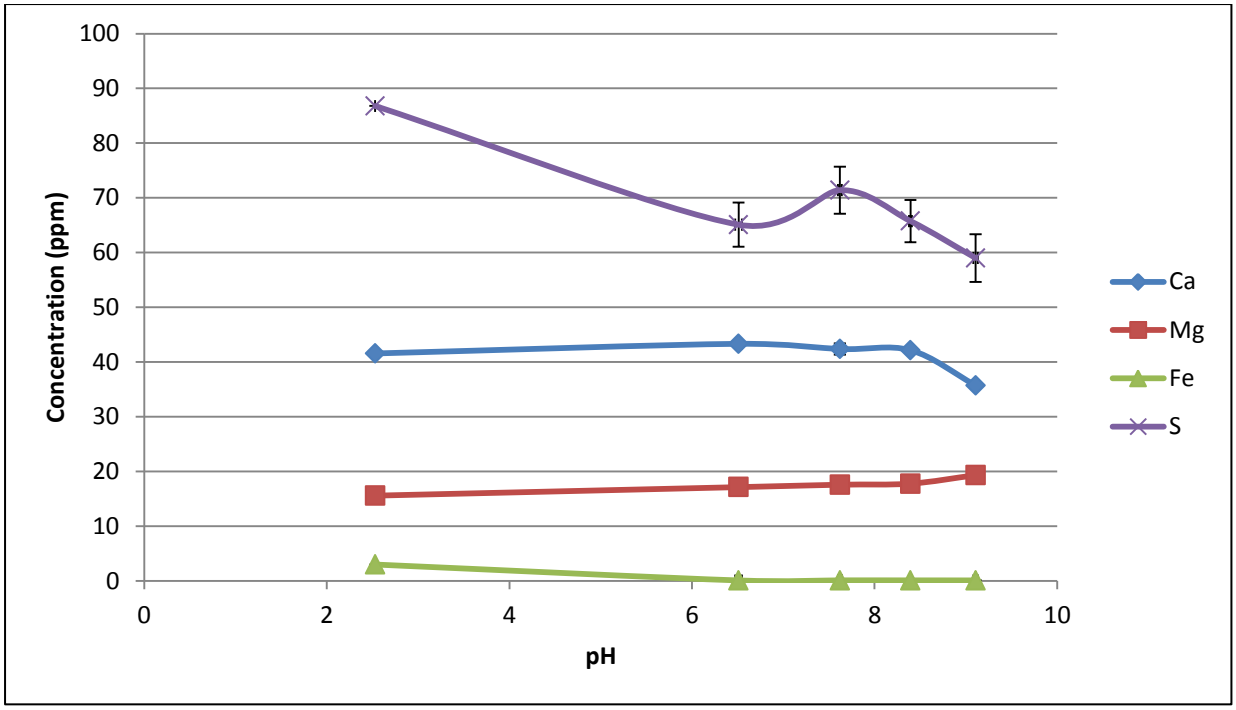

Figure 4.8: Concentrations of Ca, Mg, Fe and S* in AMD after treatment with bentonite clay at different pH levels (pH adjusted by addition of magnesium hydroxide) *S = SO_4^{2-}

As before, the initial concentrations for the elements are fairly low since the same AMD sample was used for the second and third experiments. The concentration of Fe in the solution decreased from 3 ppm to ≈0.1 ppm, though it cannot be confirmed that the removal thereof was as a result of bentonite adsorption, due to the low concentration.

Unlike in the first and second sets of experiments, in this experiment the concentration of Ca decreased whereas Mg concentration increased. Although the changes were not considerable, i.e. only ≈4 ppm increase for Mg and ≈5 ppm decrease for Ca, it could indicate that the Mg ions did form aqueous $MgSO_4$ in this experiment, thus causing the precipitation of $CaSO_4$. However, it is also possible that the concentration of Mg in solution increased simply because of the addition of $Mg(OH)_2$ for pH control, while the decreasing concentration of Ca ions resulted from a small amount thereof precipitating with SO_4^{2-} as gypsum.

The sulphate curve is much the same as with the previous two experiments, which indicates that the removal thereof from the AMD is largely independent of reagents used for pH adjustment. It also appears that the sulphate ions are more likely to be adsorbed onto the bentonite clay directly, rather than forming a precipitate compound with Ca ions in solution. This is based on the observation (Figure 4.8) that SO_4^{2-} concentrations decreased by ≈27 ppm while the concentration of Ca decreased by only ≈6 ppm.

4.5 Repeatability and accuracy

Although an effort is made to work as accurately as possible during experimental work, errors are sometimes inevitable during the execution of the experimental work. Based on this, it is important to know that the results which were obtained from the experimental runs are accurate and reliable. For each pH range which was tested during the experimental section, three separate tests were performed to see if the results correlate to indicate that the experimental results obtained are accurate. The results from these tests were used to calculate standard deviations for each data point which was used to set up the concentration curves (Figures 4.5, 4.6 and 4.8) shown in the results. The largest deviation obtained on the concentrations was calculated as ±53.14 ppm for the 5^{th} data point of the sulphate curve from the first experimental run (Figure 4.5). Although the value of the deviation is large, it is important to view it against the rest of the data for the curve. The sulphate curve stretches between a maximum and minimum concentration of ≈994 ppm and ≈715 ppm respectively. These concentrations are so large that, when viewed against them, 53.14 ppm is an acceptable deviation, which qualifies it to be employed in the experimental work. That therefore shows that the results obtained are accurate and reliable.

Chapter 5 : Conclusions and recommendations

The effect of pH level on the ability of bentonite clay to treat AMD water effectively, and determining whether burnt dolomite is a viable compound for pH control during AMD treatment was the topic of investigation for this project. In this chapter the most important conclusions are set out, which were made based on the experimental results. Recommendations will also be given for future projects of this kind.

5.1 Conclusions

The following conclusions were made based on the knowledge obtained from literature and the results of the experimental work:

- Adding slaked dolime to AMD is an effective way of increasing the pH thereof in order to induce precipitation of metals out of the water.
- The effective removal of contaminant elements such as Fe, S (as SO_4^{2-}), Al, Mn, P and Ni from AMD increases with higher pH levels.
- Treating AMD around pH 7 is not advised as the solution's transition from an acidic to basic state causes ion adsorption and precipitation reactions to become erratic.
- Slaked dolime is not capable of preventing gypsum scaling as the magnesium present in the dolime precipitates from the AMD solution before it can prompt the precipitation and adsorption of the gypsum onto the bentonite clay.
- By adding pure magnesium hydroxide to the AMD for pH adjustment, magnesium sulphate is able to form which leads to the removal of gypsum.
- Most of the SO_4^{2-} removed from the AMD is believed to be as a result of bentonite clay adsorption. The amount of SO_4^{2-} leaving the solution due to gypsum precipitation is minute as there is no significant change in the concentration of Ca^{2+} to indicate that gypsum precipitation occurs to a larger extent.

5.2 Recommendations

The following recommendations are made for any future projects or studies which may be similar to, or based upon, this project:

- The pH ranges at which the experiments were performed should be narrowed so that the effects of pH can be studied in greater detail.
- The analysis of the bentonite clay (Table 2.3) showed that 52% of its weight is made up by silica (SiO_2). This means that nearly half of the bentonite added to the AMD

during treatment is actually silica which has no adsorption abilities and is thus of no use. A study should be done regarding the removal of silica from the bentonite to yield clay with a higher adsorption capacity per weight unit.

- The mixing of bentonite with $Ca(OH)_2$, $CaCO_3$ and certain metal compounds such as $FeCl_3$ to create polymers for AMD treatment, as discussed by Ntwampe *et al.* (2015), is an interesting method which should be studied further.

References

Agnello, V.N., 2005. *Bentonite, pyrophyllite and talc in the Republic of South Africa*. Pretoria: Department of Minerals and Energy. Directorate: Mineral Economics.

Aubé, B., 2004. *The Science of Treating Acid Mine Drainage and Smelter Effluents*. [Online] Available at: http://www.infomine.com/publications/docs/Aube.pdf [Accessed 3 October 2015].

Bhattacharyya, K.G. & Gupta, S.S., 2008. Adsorption of a few heavy metals on natural and modified kaolinite and montmorillonite: A review. *Advances in Colloid and Interface Science*, 140, pp.114-31.

Brink, M.C., 2009. Purification of Water – Greenmont Method. (Patent: RSA 2008/06195).

Brink, M.C., 2012. The eradication and rehabilitation of the effects of acid mine drainage (AMD). (Patent: RSA 56169ZAOO).

Chromatography Today, 2014. *Adsorption, Absorption and Desorption — What's the Difference*. [Online] Available at: http://www.chromatographytoday.com/news/hplc-uhplc-lc-ms/31/breaking_news/adsorption_absorption_and_desorption_whats_the_difference/31397/ [Accessed 11 November 2015].

Coetzee, H., 2009. *Overview of acid mine drainage impacts in the West Rand Goldfield*. Presentation to Director General of DWAF. Department of Water Affairs.

Coetzee, H., Winde, F. & Wade, P.W., 2006. ISBN. 1770054197 *An assessment of sources, pathways, mechanisms and risks of current and potential future pollution of water and sediments in gold-mining areas of the Wonderfonteinspruit catchment*. Pretoria: Water Research Commission.

Culgor, D., 2014. *The Common Ion Effect and Altering Solubility*. [Online] Available at: http://www.colgurchemistry.com/ [Accessed 2 November 2015].

de Pable, L., Chavez, M.L. & Abatal, M., 2011. Adsorption of heavy metals in acid to alkaline environments by montmorillonite and Ca-montmorillonite. *Chemical Engineering Journal*, 171, pp.1276-86.

De Pablo, L., Chavez, M.L. & Abatal, M., 2011. Adsorption of heavy metals in acid to alkaline environments by montmorillonite and Ca-montmorillonite. *Chemical Engineering Journal*, 171, pp.1276-86.

Earthlife Africa, 2015. *Acid Mine Drainage*. [Online] Available at: http://earthlife.org.za/campaigns/acid-mine-drainage/ [Accessed 12 March 2015].

Enslin, F., 2009. *Suurloging van smaarmetaal gelaaide bentoniet*. Bachelor Thesis. Potchefstroom: Faculty of Engineering North-West University.

Enslin, F., van der Mey, L. & Waanders, F., 2010. Acid leaching of heavy metals from bentonite clay, used in the cleaning of acid mine drainage. *The Journal of The Southern African Institute of Mining and Metallurgy*, 110, pp.187-91.

Envirofluid, 2014. *How to remove Limescale for Pumps & Pipes*. [Online] Available at: https://envirofluid.com/case-studies/how-to/how-to-remove-limescale-pumps-pipes [Accessed 4 November 2015].

European Bentonite Producers Association, 2015. *Bentonite*. [Online] IMA Europe Available at: http://www.ima-europe.eu/about-industrial-minerals/industrial-minerals-ima-europe/bentonite [Accessed 6 November 2015].

Ewart, T.I., 2011. *Acid mine drainage in the Gauteng province of South Africa – A phenomenological study on the degree of alignment between stakeholders concerning a sustainable solution to acid mine drainage*. Master Thesis. Stellenbosch: University of Stellenbosch.

Gitari, W.M., Kaseke, C. & Nkuzani, B.B., 2011. Passive Remediation of Acid Mine Drainage using Bentonite Clay: A Laboratory Batch Experimental Study. *Mine Water – Managing the Challenges*, pp.325-30.

Gregory, J. & Duan, J., 2001. Hydrolyzing metal salts as coagulants. *Pure Applied Chemistry*, 73(12), pp.2017-23.

Gu, X., Evans, L.J. & Barabash, S.J., 2010. Modeling the adsorption of Cd (II), Cu (II), Ni (II), Pb (II) and Zn (II) onto montmorillonite. *Geochimica et Cosmochimica Acta*, 74, pp.5718-28.

Heviánková, S., Bestová, I. & Kyncl, M., 2014. The application of wood ash as a reagent in acid mine drainage. *Minerals Engineering*, 56, pp.109-11.

Hou, X. & Jones, B.T., 2000. Inductively Coupled Plasma/Optical Emission Spectrometry. In R.A. Meyers, ed. *Encyclopedia of Analytical Chemistry*. Chichester: John Wiley & Sons Ltd. pp.9468-85.

Ijagbemi, C.O., Baek, M. & Kim, D., 2010. Adsorptive performance of un-calcined sodium exchanged and acid modified montmorillonite for Ni2+ removal: Equilibrium, kinetics, thermodynamics and regeneration studies. *Journal of Hazardous Materials*, 174, pp.746-55.

Ikhsan, J., Wells, J.D., Johnson, B.B. & Angove, M.J., 2005. Surface complexation modeling of the sorption of Zn(II) by montmorillonite. *Colloids and Surfaces A: Physicochem. Eng. Aspects*, 252, pp.33-41.

Ispat Digest, 2014. *Lime and Calcined Dolomite for use in steel plants*. [Online] Available at: http://ispatguru.com/lime-and-calcined-dolomite-for-use-in-steel-plant/ [Accessed 20 October 2015].

Jennings, S.R., Neuman, D.R. & Blicker, P.S., 2008. *Acid Mine Drainage and Effects on Fish Health and Ecology: A Review*. Bozeman, Montana: Reclamation Research Group Publication U.S. Fish and Wildlife Service, Anchorage Fish and Wildlife Field Office.

Kearney, L., 2012. *Mining and minerals in South Africa*. [Online] Available at: http://www.southafrica.info/business/economy/sectors/mining.htm#.Vjjw-iuK8Qo [Accessed 1 March 2015].

Khalili, F.I., Salameh, N.H. & Shaybe, M.M., 2013. Sorption of Uranium(VI) and Thorium(IV) by Jordanian Bentonite. *Journal of Chemistry*, 2013.

King, H., 2015. *Dolomite*. [Online] Available at: http://geology.com/rocks/dolomite.shtml [Accessed 20 October 2015].

Lhoist, 2015. *Lime and minerals in your daily life*. [Online] Available at: http://www.lhoist.com/lime-and-minerals-your-daily-life [Accessed 5 November 2015].

Lu, P. et al., 2011. Lead coprecipitation with iron oxyhydroxide nano-particles. *Geochimica et Cosmochimica*, 75, pp.4547-61.

Maicaneanu, A., Bedelean, H., Ardelean, M. & Burca, S., 2013. Hanes and Valea Vinului (Romania) closed mines Acid Mine Drainages (AMDs) – Actual condition and passive treatment remediation proposal. *Chemosphere*, 93, pp.1400-05.

McCarthy, T.S., 2011. The Impact of Acid Mine Drainage in South Africa. *South African Journal of Science*, 107.

McCarthy, T.S., Steyl, G., Maree, J. & Zhao, B., 2010. *Mine Water Management in the Witwatersrand Gold Fields With Special Emphasis on Acid Mine Drainage*. Inter-Ministerial

Report. Johannesburg: Inter-Ministerial Committee on Acid Mine Drainage Council for Geoscience.

Metcalf, W. & Eddy, C., 2003. *Wastewater Engineering*. 4th ed. New York: McGraw-Hill Inc.

Minerals Zone, 2014. *Dolomite*. [Online] Available at: http://www.mineralszone.com/minerals/dolomite.html [Accessed 21 October 2015].

Montaser, A., 1998. *Inductively Coupled Plasma Mass Spectrometry*. Washington D.C.: Wiley.

Nel, M., Waander, F.B. & Fosso-Kankeu, E., 2014. *Adsorption potential of bentonite and attapulgite clays applied for the desalination of sea water*. Conference Report. Cape Town: 6th International Conference on Green Technology, Renewable Energy & Environmental Engineering North-West University.

Ntwampe, I.O., Waanders, F.B. & Bunt, T.S., 2015. Comparison between mixing and shaking techniques during the destabilization-hydrolysis of the acid mine drainage (AMD) using Ca(OH)2 and Mg(OH)2. *Journal of Chemical Engineering and Materials Science*, 6(3), pp.15-33.

Oelofse, S. & Strydom, W., 2010. ISBN: 978-0-7988-5595-2 *A CSIR Perspective on Water in South Africa*. Johannesburg: CSIR Council for Scientific and Industrial Research.

Scott, R., 1995. ISBN. 1868451747 *Flooding of Central and East Rand Gold Mines: An Investigation Into Controls Over the Inflow Rate, Water Quality and the Predicted Impacts of Flooded Mines*. Research Report. Bloemfontein: University of the Orange Free State Institute for Groundwater Studies.

South African Department of Water & Sanitation, 2015. *Witwatersrand, Gauteng: Acid Mine Drainage: Long Term Solution*. [Online] Available at: https://www.dwaf.gov.za/Projects/AMDFSLTS/default.aspx [Accessed 12 March 2015].

Strawn, D.G. & Sparks, D.L., 1999. The Use of XAFS to Distinguish between Inner- and Outer-Sphere Lead Adsorption Complexes on Montmorillonite. *Journal of Colloid and Interface Science*, 216, pp.257-69.

Van der Wat, J.G., 2011. *Desorption of rare earth elements from bentonite clay via acid leaching*. Bachelor Thesis. Potchefstroom: Faculty of Engineering North-West University.

Vermeulen, U., 2012. *Desorption of heavy metals from Bentonite clay by means of sulphuric acid addition*. Bachelor Thesis. Potchefstroom: Faculty of Engineering North-West University.

William, S., Herring, F.G., Madura, J.D. & Petrucci, R.H., 2007. Common-Ion Effect in Solubility Equilibria. In *General Chemistry Principles and Modern Applications*. 9th ed. New Jersay: Prentice Hall.

Wolf, R.E., 2005. *What is ICP-MS? And more importantly, what can it do?* [Online] Available at: http://crustal.usgs.gov/laboratories/icpms/intro.html [Accessed 08 November 2015].

Wu, P., Zhang, Q., Dai, Y. & Zhu, N., 2011. Adsorption of Cu(II), Cd(II) and Cr(III) ions from aqueous solutions on humic acid modified Ca-montmorillonite. *Geoderma*, 164, pp.215-19.

Xu, D., Zhou, X. & Wang, X., 2008. Adsorption and desorption of Ni2+ on Na-montmorillonite: Effect of pH, ionic strength, fulvic acid, humic acid and addition sequences. *Applied Clay Science*, 39, pp.133-41.

Yellowstar Bentonite, 2015. *Yellowstar Bentonite*. [Online] Available at: http://www.yellowstarmining.co.za/index.html [Accessed 5 October 2015].

Zinck, J., 2005. *Review of Disposal, Reprocessing and Reuse Options for Acidic Drainage Treatment Sludge*. Government Report. Canada: Natural Resources Canada The Mining Association of Canada.

Appendix A: AMD sample analysis results

Table A.1: AMD Sample 1 analysis results showing elements present and their concentrations (Measured in ppm)

Element	Concentration
Ag 328.068	0.01859
Al 396.152	3.06548
As 188.980	0.00000
Ba 455.403	0.03111
Be 313.107	0.01430
Ca 422.673	543.468
Cd 226.502	0.22919
Co 230.786	0.61956
Cr 267.716	0.00000
Cu 327.395	0.34059
Fe 259.940	118.094
K 766.491	12.7852
Li 670.783	0.15165
Mg 280.270	182.579
Mn 257.610	108.599
Mo 202.032	0.00000
Na 588.995	109.825
Ni 231.604	2.33580
P 213.618	2.82344
Pb 220.353	0.66043
Pb 283.305	1.44170
S 182.562	993.484
Sb 206.834	5.88847
Se 196.026	0.00000
Sr 407.771	0.49233
Tl 276.789	2.58305
Tl 351.923	0.00000
V 292.401	0.00665
Zn 213.857	1.58912

Table A.2: AMD Sample 2 analysis results showing elements present and their concentrations (Measured in ppm)

Element	Concentration
Ag 328.068	0.00362
Al 396.152	0.13980
As 188.980	0.17872
Ba 455.403	0.00300
Be 313.107	0.00100
Ca 422.673	41.5694
Cd 226.502	0.00970
Co 230.786	0.16847
Cr 267.716	0.02615
Cu 327.395	0.00848
Fe 259.940	3.00127
K 766.491	1.05640
Li 670.783	0.00776
Mg 280.270	15.5862
Mn 257.610	7.02532
Mo 202.032	0.10977
Na 588.995	10.0401
Ni 231.604	0.06486
P 213.618	0.09598
Pb 220.353	0.37560
Pb 283.305	0.12712
S 182.562	86.7855
Sb 206.834	0.36865
Se 196.026	0.87345
Sr 407.771	0.05112
Tl 276.789	0.04455
Tl 351.923	0.10470
V 292.401	0.00495
Zn 213.857	0.03689

Appendix B: ICP-OES Results for 1st experimental run (Using slaked dolime)

Table B.1: ICP-OES Results for supernatant samples recovered from 1st experimental run showing element concentrations (All concentrations measured in ppm)

pH range	6-7			Average	7-8			Average	8-9				Average
Sample #	13	14	15		30	29	31		16	17	20	18	
pH	6.63	6.65	6.84	6.71	7.3	7.31	7.32	7.31	8.71	8.81	8.84	8.85	8.80
Element													
Ag 328.068	0.0380	0.0132	0.0007	0.0173	0.0000	0.0000	0.0324	0.0108	0.0059	0.0279	0.0076	0.0100	0.0128
Al 396.152	0.5207	0.5088	0.4670	0.4988	0.3366	0.4972	0.6025	0.4787	0.2139	0.1748	0.3785	0.2576	0.2562
As 188.980	0.0000	0.0000	0.0000	0.0000	0.0000	0.0000	0.0000	0.0000	0.0000	0.0000	0.0000	0.0000	0.0000
Ba 455.403	0.0712	0.0744	0.0730	0.0729	0.0541	0.0704	0.0729	0.0658	0.0531	0.0635	0.0613	0.0698	0.0619
Be 313.107	0.0044	0.0051	0.0036	0.0044	0.0012	0.0024	0.0000	0.0012	0.0026	0.0076	0.0070	0.0039	0.0053
Ca 422.673	602.25	621.39	630.74	618.13	586.61	570.65	585.66	580.97	627.31	640.13	666.57	643.56	644.39
Cd 226.502	0.1783	0.1901	0.1759	0.1814	0.0926	0.1096	0.1164	0.1062	0.2042	0.2056	0.2158	0.1815	0.2018
Co 230.786	0.3550	0.0864	0.2163	0.2192	0.3569	0.3819	0.0000	0.2462	0.3791	0.0929	0.0966	0.1570	0.1814
Cr 267.716	0.0440	0.0000	0.0000	0.0147	0.0245	0.0000	0.0602	0.0282	0.0035	0.0279	0.0056	0.0000	0.0092
Cu 327.395	0.3038	0.2837	0.2576	0.2817	0.2613	0.2959	0.2522	0.2698	0.2807	0.2912	0.2895	0.2764	0.2844
Fe 259.940	0.8142	0.9950	0.6800	0.8298	0.5532	1.0154	0.7097	0.7594	0.4276	0.7923	3.0720	0.4757	1.1919
K 766.491	12.135	12.615	13.230	12.660	11.538	11.628	11.763	11.643	12.680	12.025	11.760	12.080	12.136
Li 670.783	0.1335	0.1352	0.1358	0.1348	0.1291	0.1250	0.1262	0.1268	0.1316	0.1291	0.1195	0.1311	0.1278
Mg 280.270	200.25	194.92	194.75	196.64	205.24	200.57	203.01	202.94	187.50	185.13	169.98	185.68	182.07
Mn 257.610	68.953	63.726	59.541	64.073	67.787	70.538	63.766	67.364	31.479	21.797	26.202	21.123	25.150
Mo 202.032	0.2539	0.2669	0.3077	0.2762	0.5030	0.7540	0.0000	0.4190	0.9294	0.3663	0.5987	0.1997	0.5235
Na 588.995	105.68	107.15	107.42	106.75	100.75	99.385	99.867	100.00	104.14	104.43	99.35	103.19	102.78
Ni 231.604	1.5442	1.5804	0.9792	1.3679	1.0083	1.7648	1.3789	1.3840	0.8882	0.1820	0.6387	0.7176	0.6066
P 213.618	2.1042	2.2743	2.1052	2.1612	1.9687	2.0860	2.0223	2.0257	1.5039	1.6855	1.5991	1.7441	1.6331
Pb 220.353	1.6126	1.0283	0.0497	0.8969	0.0000	0.3147	0.4441	0.2529	0.7688	0.0000	0.2889	0.0000	0.2644
Pb 283.305	0.7116	0.4846	1.2678	0.8214	0.5932	0.0000	1.5517	0.7150	0.0690	0.1240	0.5174	0.3903	0.2752
S 182.562	738.16	760.37	750.86	749.80	802.74	844.95	847.22	831.64	804.34	838.44	834.90	752.52	807.55
Sb 206.834	3.5402	3.3001	3.3375	3.3926	3.0365	2.1272	2.2328	2.4655	2.8798	2.8896	2.5480	2.2968	2.6535
Se 196.026	0.0000	0.0000	0.0000	0.0000	0.0000	0.0000	0.0000	0.0000	0.0000	0.0000	0.0000	0.0000	0.0000
Sr 407.771	0.5353	0.5529	0.5602	0.5495	0.5603	0.5540	0.5532	0.5558	0.5473	0.5566	0.5197	0.5422	0.5415
Tl 276.789	3.4440	1.2818	8.6763	4.4673	1.0623	3.9909	0.0000	1.6844	5.1757	5.6572	3.2595	5.3875	4.8700
Tl 351.923	0.0000	0.0000	0.0000	0.0000	0.0000	0.0000	0.0000	0.0000	0.0000	0.0000	0.0000	0.0000	0.0000
V 292.401	0.0126	0.0000	0.0259	0.0129	0.0169	0.0451	0.0542	0.0387	0.0241	0.0000	0.0575	0.0803	0.0405
Zn 213.857	0.7716	0.7000	0.4450	0.6389	0.4584	0.8100	0.8311	0.6998	0.2804	0.4120	0.5572	0.5995	0.4623

Table B.2: ICP-OES Results for supernatant samples recovered from 1st experimental run showing element concentrations (Continued)

pH range	9-10			Average	10-11				Average	11-12			Average
Sample #	32	28	19		21	27	25	26		23	24	22	
pH	9.27	9.32	9.57	9.39	10.36	10.64	10.8	10.81	10.65	11.05	11.24	11.42	11.24
Element													
Ag 328.068	0.0049	0.0685	0.0170	0.0301	0.0266	0.0001	0.0513	0.0000	0.0195	0.0758	0.0000	0.0000	0.0253
Al 396.152	0.1376	0.1874	0.2722	0.1991	0.1941	0.2490	0.2725	0.2551	0.2427	0.2072	0.3291	0.1975	0.2446
As 188.980	0.0000	0.0000	0.0000	0.0000	0.0000	0.0000	0.000	0.0000	0.0000	0.0000	0.0000	0.0000	0.0000
Ba 455.403	0.0327	0.0376	0.0631	0.0445	0.0618	0.0574	0.0609	0.0564	0.0591	0.0600	0.0602	0.0578	0.0593
Be 313.107	0.0000	0.0010	0.0048	0.0019	0.0000	0.0034	0.0056	0.0031	0.0030	0.0051	0.0044	0.0017	0.0038
Ca 422.673	673.69	696.91	738.21	702.94	783.60	762.97	719.70	790.95	764.31	842.52	833.16	793.85	823.17
Cd 226.502	0.1706	0.1582	0.1985	0.1758	0.1691	0.2039	0.1840	0.2075	0.1911	0.1819	0.2168	0.1865	0.1951
Co 230.786	0.0000	0.0990	0.0284	0.0425	0.0000	0.1680	0.1600	0.0408	0.0922	0.2208	0.0880	0.1232	0.1440
Cr 267.716	0.0399	0.0000	0.0000	0.0133	0.0176	0.0008	0.0000	0.0546	0.0183	0.1073	0.0131	0.0000	0.0401
Cu 327.395	0.2669	0.2378	0.2921	0.2656	0.3002	0.2665	0.2572	0.2505	0.2686	0.3179	0.2955	0.3000	0.3045
Fe 259.940	2.8059	0.3790	0.6849	1.2899	0.5468	0.5527	0.5201	0.4434	0.5158	0.3453	0.5331	0.5603	0.4796
K 766.491	11.680	11.372	11.595	11.549	11.561	11.413	11.277	11.259	11.377	11.836	11.082	11.334	11.417
Li 670.783	0.1232	0.1185	0.1233	0.1217	0.1203	0.1197	0.1173	0.1172	0.1186	0.1185	0.1157	0.1152	0.1164
Mg 280.270	154.42	155.03	149.37	152.94	75.422	74.261	68.154	66.741	71.145	19.516	15.083	13.330	15.976
Mn 257.610	6.2648	5.7640	0.8533	4.2940	0.1352	0.1754	0.1082	0.1056	0.1311	0.0731	0.0772	0.1141	0.0881
Mo 202.032	1.1778	0.1483	0.0000	0.4420	0.0000	0.0000	0.0541	0.2901	0.0861	0.2890	0.0313	0.0414	0.1206
Na 588.995	99.725	98.450	101.06	99.75	100.18	101.32	99.396	100.48	100.34	100.90	98.77	102.00	100.56
Ni 231.604	0.6874	1.4397	0.4836	0.8702	0.3943	1.1047	0.8949	0.8421	0.8090	0.4438	0.7764	0.3417	0.5206
P 213.618	1.6067	1.4600	1.4503	1.5057	1.2996	1.4297	1.3441	1.2508	1.3310	1.2650	1.3987	1.2695	1.3111
Pb 220.353	0.9733	0.0000	0.0000	0.3244	1.2651	0.6057	0.9476	0.2835	0.7755	0.1882	1.3659	0.5375	0.6972
Pb 283.305	0.1820	0.1304	0.3586	0.2237	0.5745	0.9015	0.4215	0.3621	0.5649	0.4154	0.4220	0.0000	0.2791
S 182.562	837.82	742.13	749.89	776.61	749.09	742.39	760.56	735.82	746.96	722.04	728.80	694.20	715.02
Sb 206.834	2.3062	1.9486	1.9767	2.0772	4.0740	4.0545	3.4278	3.6694	3.8064	4.4365	3.1811	3.4735	3.6970
Se 196.026	0.0000	0.0000	0.0000	0.0000	0.0000	0.0000	0.0000	0.0000	0.0000	0.0000	0.0000	0.0000	0.0000
Sr 407.771	0.5528	0.5405	0.5208	0.5380	0.5305	0.5204	0.5141	0.5199	0.5212	0.5147	0.5115	0.5033	0.5098
Tl 276.789	8.9265	2.0727	0.5559	3.8517	0.0000	0.4045	0.2149	1.4135	0.5082	0.0000	0.3612	0.0000	0.1204
Tl 351.923	0.0000	0.0000	0.0000	0.0000	0.0000	0.0000	0.0000	0.0000	0.0000	0.0000	0.0000	0.0000	0.0000
V 292.401	0.0101	0.0690	0.0000	0.0264	0.0000	0.0000	0.0000	0.0488	0.0122	0.0623	0.0217	0.0000	0.0280
Zn 213.857	0.6280	0.3250	0.5614	0.5048	0.5800	0.3257	0.2062	0.4832	0.3988	0.2803	0.6359	0.6397	0.5186

Appendix C: ICP-OES Results for 2nd experimental run (Using calcium hydroxide)

Table C.1: ICP-OES Results for supernatant samples recovered from 2nd experimental run showing element concentrations (All concentrations measured in ppm)

pH Range	6-7			Average	7-8			Average
Sample #	40	41	42		46	47	48	
pH	6.5	6.67	6.84	6.67	7.52	7.54	7.58	7.55
Element								
Ag 328.068	0.0019	0.0024	0.0003	0.0016	0.0008	0.0000	0.0000	0.0003
Al 396.152	0.1872	0.1490	0.1401	0.1588	0.1531	0.1575	0.1761	0.1622
As 188.980	0.2152	0.5785	0.0740	0.2892	0.1632	0.0000	0.0987	0.0873
Ba 455.403	0.0195	0.0161	0.0161	0.0172	0.0157	0.0155	0.0141	0.0151
Be 313.107	0.0002	0.0000	0.0003	0.0002	0.0000	0.0000	0.0001	0.0000
Ca 422.673	51.597	51.616	51.991	51.735	49.889	49.660	49.318	49.622
Cd 226.502	0.0034	0.0030	0.0062	0.0042	0.0027	0.0139	0.0002	0.0056
Co 230.786	0.0000	0.0000	0.0000	0.0000	0.0000	0.0000	0.0000	0.0000
Cr 267.716	0.0000	0.0105	0.0060	0.0055	0.0009	0.0144	0.0109	0.0087
Cu 327.395	0.0260	0.0068	0.0085	0.0138	0.0078	0.0072	0.0067	0.0072
Fe 259.940	0.1217	0.1059	0.0769	0.1015	0.1171	0.1309	0.0992	0.1157
K 766.491	2.1213	1.2899	1.2995	1.5703	1.3341	1.3363	1.3237	1.3314
Li 670.783	0.0079	0.0078	0.0079	0.0079	0.0080	0.0080	0.0080	0.0080
Mg 280.270	12.882	12.795	12.609	12.762	13.074	13.013	13.039	13.042
Mn 257.610	2.8866	2.8823	2.6724	2.8138	4.3040	4.4712	4.3119	4.3623
Mo 202.032	0.0185	0.0738	0.0617	0.0513	0.1407	0.0384	0.1468	0.1086
Na 588.995	12.296	12.160	12.110	12.188	12.404	12.400	12.284	12.363
Ni 231.604	0.0600	0.0305	0.0100	0.0335	0.0663	0.0275	0.0299	0.0412
P 213.618	0.0422	0.0438	0.0535	0.0465	0.0124	0.0185	0.0201	0.0170
Pb 220.353	0.0000	0.0199	0.0000	0.0066	0.0000	0.0000	0.0000	0.0000
Pb 283.305	0.0000	0.0198	0.0000	0.0066	0.0000	0.0108	0.0187	0.0098
S 182.562	65.932	60.513	72.516	66.320	70.646	75.740	62.695	69.694
Sb 206.834	0.4126	0.0000	0.0967	0.1698	0.2645	0.0615	0.0000	0.1087
Se 196.026	0.9599	0.1903	0.5292	0.5598	0.1797	1.0609	0.8236	0.6881
Sr 407.771	0.0683	0.0684	0.0668	0.0679	0.0685	0.0687	0.0694	0.0689
Tl 276.789	0.0644	0.0778	0.0655	0.0692	0.1009	0.0000	0.1926	0.0978
Tl 351.923	0.0413	0.0000	0.0000	0.0138	0.0000	0.0000	0.0000	0.0000
V 292.401	0.0061	0.0000	0.0000	0.0020	0.0017	0.0015	0.0000	0.0011
Zn 213.857	0.0073	0.0116	0.0080	0.0089	0.0196	0.0116	0.0144	0.0152

Table C.2: ICP-OES Results for supernatant samples recovered from 2nd experimental run showing element concentrations (Continued)

pH Range	8-9			Average	9-10			Average
Sample #	43	44	45		49	50	51	
pH	8.35	8.55	8.47	8.46	9.37	9.38	9.4	9.38
Element								
Ag 328.068	0.0040	0.0005	0.0000	0.0015	0.0004	0.0000	0.0006	0.0004
Al 396.152	0.1147	0.1320	0.1132	0.1200	0.0964	0.0930	0.1060	0.0985
As 188.980	0.0514	0.0060	0.0000	0.0000	0.1915	0.0000	0.0000	0.0638
Ba 455.403	0.0119	0.0123	0.0126	0.0123	0.0118	0.0112	0.0115	0.0115
Be 313.107	0.0002	0.0001	0.0000	0.0001	0.0002	0.0002	0.0000	0.0001
Ca 422.673	53.539	53.698	54.083	53.773	54.386	55.087	55.319	54.930
Cd 226.502	0.0036	0.0002	0.0042	0.0027	0.0000	0.0109	0.0003	0.0037
Co 230.786	0.0000	0.0000	0.0000	0.0000	0.0000	0.0000	0.0000	0.0000
Cr 267.716	0.0146	0.0067	0.0000	0.0071	0.0037	0.0000	0.0091	0.0043
Cu 327.395	0.0075	0.0113	0.0078	0.0089	0.0089	0.0064	0.0071	0.0074
Fe 259.940	0.0636	0.0915	0.0599	0.0717	0.0637	0.0513	0.0619	0.0590
K 766.491	1.2925	1.3747	1.2758	1.3143	1.2803	1.2421	1.2680	1.2634
Li 670.783	0.0075	0.0076	0.0076	0.0076	0.0075	0.0074	0.0074	0.0075
Mg 280.270	12.608	12.786	12.612	12.669	11.791	11.695	11.798	11.761
Mn 257.610	1.5746	1.6675	1.3000	1.5140	0.2779	0.2509	0.2879	0.2722
Mo 202.032	0.0530	0.0159	0.0624	0.0438	0.0000	0.0082	0.0000	0.0027
Na 588.995	12.243	12.397	12.088	12.243	11.967	12.093	12.086	12.049
Ni 231.604	0.0210	0.0101	0.0616	0.0309	0.0712	0.0083	0.0436	0.0410
P 213.618	0.0113	0.0000	0.0135	0.0082	0.0000	0.0000	0.0107	0.0036
Pb 220.353	0.3122	0.0000	0.0000	0.1041	0.0000	0.0000	0.2177	0.0726
Pb 283.305	0.0000	0.0000	0.0162	0.0054	0.0000	0.0000	0.0329	0.0110
S 182.562	63.663	70.222	69.508	67.798	60.945	58.037	65.799	61.593
Sb 206.834	0.2686	0.0000	0.3821	0.2169	0.3395	0.0000	0.0378	0.1257
Se 196.026	0.0000	0.0237	0.1169	0.0469	0.0270	0.0931	0.5736	0.2312
Sr 407.771	0.0695	0.0724	0.0683	0.0701	0.0676	0.0719	0.0711	0.0702
Tl 276.789	0.0000	0.0000	0.0895	0.0298	0.1158	0.0209	0.0084	0.0484
Tl 351.923	0.0000	0.0000	0.0000	0.0000	0.0000	0.0000	0.0000	0.0000
V 292.401	0.0051	0.0037	0.0000	0.0029	0.0060	0.0016	0.0000	0.0025
Zn 213.857	0.0202	0.0041	0.0235	0.0159	0.0174	0.0086	0.0179	0.0146

Appendix D: ICP-OES Results for 3rd experimental run (Using magnesium hydroxide)

Table D.1: ICP-OES Results for supernatant samples recovered from 3rd experimental run showing element concentrations (All concentrations measured in ppm)

pH Range	6-7			Average	7-8			Average
Sample #	52	53	54		55	56	57	
pH	6.54	6.47	6.52	6.51	7.62	7.64	7.6	7.62
Element								
Ag 328.068	0.0000	0.0050	0.0000	0.0017	0.0000	0.0109	0.0000	0.0036
Al 396.152	0.1201	0.1311	0.1364	0.1292	0.1254	0.1464	0.1299	0.1339
As 188.980	0.0000	0.1455	0.0000	0.0485	0.1274	0.0000	0.4906	0.2060
Ba 455.403	0.0163	0.0160	0.0160	0.0161	0.0158	0.0166	0.0166	0.0163
Be 313.107	0.0000	0.0002	0.0000	0.0001	0.0004	0.0000	0.0000	0.0001
Ca 422.673	43.159	43.343	43.481	43.328	41.214	43.124	42.776	42.371
Cd 226.502	0.0000	0.0000	0.0070	0.0023	0.0000	0.0000	0.0067	0.0022
Co 230.786	0.0000	0.0000	0.0000	0.0000	0.0000	0.0000	0.0000	0.0000
Cr 267.716	0.0069	0.0128	0.0220	0.0139	0.0056	0.0046	0.0000	0.0034
Cu 327.395	0.0051	0.0075	0.0071	0.0066	0.0054	0.0052	0.0064	0.0056
Fe 259.940	0.0893	0.0940	0.0952	0.0928	0.1012	0.1071	0.1393	0.1159
K 766.491	1.2796	1.2748	1.2623	1.2722	1.2142	1.2736	1.2464	1.2447
Li 670.783	0.0076	0.0078	0.0076	0.0077	0.0076	0.0076	0.0075	0.0076
Mg 280.270	17.751	16.752	16.922	17.142	17.823	17.474	17.456	17.584
Mn 257.610	5.0543	4.7971	4.8022	4.8845	4.5741	4.6568	4.6605	4.6305
Mo 202.032	0.0000	0.1134	0.0153	0.0429	0.0648	0.0140	0.0233	0.0340
Na 588.995	11.936	12.118	12.118	12.057	11.481	12.071	12.037	11.863
Ni 231.604	0.0964	0.0000	0.0145	0.0370	0.0122	0.0611	0.0441	0.0392
P 213.618	0.0696	0.0657	0.0573	0.0642	0.0424	0.0620	0.0502	0.0515
Pb 220.353	0.0065	0.2329	0.3163	0.1853	0.2381	0.0000	0.0000	0.0794
Pb 283.305	0.0000	0.0113	0.0262	0.0125	0.0363	0.0000	0.0062	0.0142
S 182.562	62.736	69.772	62.806	65.105	73.304	74.454	66.487	71.415
Sb 206.834	0.2711	0.0000	0.5144	0.2618	0.0339	0.2997	0.2641	0.1992
Se 196.026	0.8904	0.5628	0.6714	0.7082	0.2041	0.1762	0.7391	0.3731
Sr 407.771	0.0647	0.0618	0.0624	0.0630	0.0618	0.0642	0.0617	0.0626
Tl 276.789	0.1060	0.0775	0.0441	0.0759	0.1809	0.0000	0.2170	0.1326
Tl 351.923	0.0000	0.0000	0.0000	0.0000	0.0000	0.0000	0.0000	0.0000
V 292.401	0.0065	0.0064	0.0032	0.0054	0.0045	0.0006	0.0063	0.0038
Zn 213.857	0.0000	0.0000	0.0000	0.0000	0.0000	0.0000	0.0000	0.0000

Table D.2: ICP-OES Results for supernatant samples recovered from 3rd experimental run showing element concentrations (Continued)

pH Range	8-9			Average	9-10			Average
Sample #	58	59	60		61	61	63	
pH	8.41	8.39	8.38	8.39	9.11	9.08	9.13	9.11
Element								
Ag 328.068	0.0000	0.0000	0.0000	0.0000	0.0000	0.0000	0.0009	0.0003
Al 396.152	0.1243	0.1374	0.1470	0.1363	0.1302	0.1385	0.1255	0.1314
As 188.980	0.0000	0.6363	0.0841	0.2401	0.1858	0.0313	0.5758	0.2643
Ba 455.403	0.0151	0.0154	0.0157	0.0154	0.0136	0.0134	0.0129	0.0133
Be 313.107	0.0002	0.0000	0.0003	0.0002	0.0001	0.0001	0.0004	0.0002
Ca 422.673	42.623	41.944	41.904	42.157	36.062	35.512	35.651	35.742
Cd 226.502	0.0000	0.0000	0.0012	0.0004	0.0000	0.0051	0.0024	0.0025
Co 230.786	0.0000	0.0000	0.0000	0.0000	0.0000	0.0000	0.0000	0.0000
Cr 267.716	0.0027	0.0076	0.0068	0.0057	0.0023	0.0000	0.0061	0.0028
Cu 327.395	0.0070	0.0076	0.0082	0.0076	0.0048	0.0061	0.0059	0.0056
Fe 259.940	0.0963	0.1128	0.1211	0.1101	0.1029	0.1060	0.0893	0.0994
K 766.491	1.2768	1.2410	1.2431	1.2536	1.1260	1.1088	1.0607	1.0985
Li 670.783	0.0075	0.0077	0.0079	0.0077	0.0064	0.0067	0.0065	0.0065
Mg 280.270	17.760	17.741	17.834	17.779	19.380	19.435	19.180	19.331
Mn 257.610	4.4757	4.4901	4.5668	4.5109	3.4540	3.4442	3.0468	3.3150
Mo 202.032	0.0642	0.0084	0.1236	0.0654	0.2047	0.0000	0.2322	0.1456
Na 588.995	11.936	11.758	11.669	11.788	10.034	9.8869	9.9457	9.9556
Ni 231.604	0.0822	0.0635	0.0349	0.0602	0.0071	0.0058	0.0000	0.0043
P 213.618	0.0321	0.0357	0.0407	0.0362	0.0248	0.0262	0.0398	0.0303
Pb 220.353	0.0000	0.0000	0.1354	0.0451	0.0509	0.1456	0.1216	0.1061
Pb 283.305	0.0000	0.0000	0.0000	0.0000	0.0277	0.0800	0.0124	0.0400
S 182.562	62.239	69.908	65.125	65.757	57.885	55.334	63.819	59.013
Sb 206.834	0.4268	0.3881	0.0317	0.2822	0.0074	0.3303	0.0230	0.1203
Se 196.026	0.0000	0.0000	0.2069	0.0690	0.0798	0.1595	0.2280	0.1558
Sr 407.771	0.0620	0.0622	0.0605	0.0616	0.0558	0.0572	0.0518	0.0549
Tl 276.789	0.9326	0.4814	0.0492	0.4877	1.0622	0.9546	0.3743	0.7970
Tl 351.923	0.0000	0.0000	0.0000	0.0000	0.0000	0.0000	0.0000	0.0000
V 292.401	0.0080	0.0056	0.0000	0.0046	0.0046	0.0000	0.0000	0.0015
Zn 213.857	0.0000	0.0000	0.0000	0.0000	0.0000	0.0000	0.0000	0.0000